UNIVERSITY OF SOUTHERN CALIFORNIA

DEPARTMENT OF CIVIL ENGINEERING

CURRENT DEVELOPMENTS IN DATA PROCESSING OF STRONG MOTION ACCELEROGRAMS

by

Vincent W. Lee and Mihailo D. Trifunac

Report No. 84-01

Los Angeles, California 90089

August 1984

CHAPTER I

Data Processing of Strong Motion Accelerograms

1.1 Introduction

The first strong motion earthquake accelerogram was recorded on March 10, 1933 during the Long Beach, California earthquake. This remarkable pioneering accomplishment, recently commemorated during the 50th Anniversary of Strong Motion Seismology in Los Angeles (Hudson 1984) marks the beginning of this young applied science. Through the 1940's and 1950's the network of strong motion accelerogram stations in California grew slowly producing only a dozen or so significantly strong accelerograms (Alford et al, 1951). The accelerograph data processing of that time required lengthy manual calculations (Housner, 1947) or analog computer calculations suitable only for a small number of records (Biot, 1941). With rapid growth of the number of the recording stations in the mid 1960's and the development and availability of digital computers the new methods associated with digital data processing slowly gained in speed, accuracy, access and popularity (Brady 1966). However, it was not until the late 1960's and early 1970's that the large number of recorded accelerograms and the need of many investigators to compare their results on a common basis necessitated a systematic development of routine data processing of strong motion accelerograms.

In general, the principles and requirements governing routine data processing of strong motion records have changed little if any since the early 1970's (Trifunac and Lee 1973). However, during the last decade we have witnessed a remarkable progress in digital signal processing techniques, in their accuracy, efficiency and speed. The aim of this

work is to show what improvements have been incorporated into the routine data processing of strong motion accelerograms so far and what principles and constraints should govern future work.

1.2 Previous Work

The early systematic development of routine computer programs for processing strong-motion earthquake accelerograms was initiated with funding from the National Science Foundation (NSF) in the late 1960's, and was completed in the early part of the 1970's (Trifunac and Lee, 1973). Almost all of the earthquake signals then were only available on analog films. Digital accelerograph data were obtained from the analog films by digitizing the records manually. For example, all of the February 9, 1971 San Fernando Earthquake records have been digitized using a Benson-Lehner 099D hand operated digitizer. Each record in its enlarged form was first placed on the digitizing table with horizontal axis lined up by eye to an estimated zero axis. Each trace was then digitized by placing the cross-hair manually on successive x-y coordinates of the trace. The digitizer converted the coordinates by digital figures, which were subsequently transferred to cards. The traces were digitized on an unequal time basis to ensure the best definition of the trace for a given number of data points. The average number of points per second of a typical trace of the record was about 20 to 30 points in general and up to about 30 to 50 points in the most oscillating sections of the trace.

The routine data processing software developed with this digitization scheme then (Trifunac and Lee, 1973) consists of the following steps:

(I) Volume I Processing:

The timing marks are first checked for "evenness" of spacing, and then smoothed by the 1/4, 1/2, 1/4 running average. The x coordinates of each trace are then scaled to units of time in seconds. Each fixed trace (baseline) is next smoothed and subtracted from the corresponding acceleration trace, with the y coordinates subsequently scaled to units of G/10.

(II) Volume II Processing:

The scaled uncorrected Vol. I acceleration data are next corrected for instrument frequency response and baseline adjustment. The data are first lowpass filtered with an Ormsby filter having a cutoff frequency f_C = 25 Hz and a roll-off termination frequency f_T = 27 Hz. Instrument correction is next performed using the instrument constants. These constants are respectively the natural frequency and ratio of critical damping of the instrument considered as a single-degree-of-freedom system. Those are determined from calibration tests for each accelerograph transducer. The data are then baseline corrected by a highpass Ormsby filter. The cutoff and roll-off frequencies of the filter are usually determined from the signal-to-noise ratio of each component (Trifunac and Lee, 1978). The accelerogram data are then integrated twice to get the velocity and displacement data. To avoid long period errors resulting from the uncertainties involved in estimating the initial values of velocity and displacement, the computed velocity and displacement data are highpass filtered at each stage of integration, using the Ormsby filter with the same cutoff and roll-off frequencies as for the corrected accelerogram.

(III) Volume III Processing:

Using an approach based on the exact analytical solution of the Duhamel integral for successive linear segments of excitation, this stage consists of calculating the Response and Fourier Spectra for 91 periods and 5 dampings from the Vol. II corrected accelerogram data, the times of maximum response for all periods and dampings are also recorded.

The development of the Automatic Routine Digitization System (ARDS) at USC has now been completed (Trifunac and Lee, 1979). Accelerogram data are now digitized automatically at 200 points per second by this system, using a Photodensitometer Photoscan P-1000 by Optronics International. A sampling period of .005 seconds means that data up to a Nyquist frequency of 100 Hz are now available. The digitized data are directly stored on disk on the Nova 3 computer after digitization and editing. The above routine computer processing programs are also available on the mini-computer and can be used to process the data directly (Lee and Trifunac, 1979 II).

1.3 The Updated System

Following the recent upgrading of the digitization hardware systems, and the advances in the theory of digital signal analysis, the routine data processing of strong-motion accelerograms has been upgraded to improve the accuracy and efficiency of the performance of the entire system.

The work to be presented in the subsequent chapters can be divided into the following steps:

Step I: Design of Lowpass Digital Filters

Chapter II will study the availability, characteristics, properties and efficiencies of digital filters for low-, high- and band-pass digital filters in general. Much of the attention will be paid to lowpass filters since those provide the essential relations for deriving either of the other two types. The problem associated with the design of the digital lowpass filter to simulate an ideal lowpass filter will first be discussed. The different types of lowpass filters available in literature will then be examined and compared. A guideline for the design and improvement of new and/or existing lowpass filters is then considered, followed by a proposed example of a lowpass filter designed within the proposed guidelines.

Step II: Design of the Differentiating Filter

Numerical Differentiation is required in the step of Instrument Correction. Instrument correction represents the step of the transformation from the digitized relative displacement of transducer x(t) to the true input ground acceleration a(t). The ideal differentiating filter is first examined, and the problems associated with its design are discussed. The different types of differentiating filters available are examined and their performance evaluated. A guideline for the design of the filter for instrument correction in earthquake engineering is then considered, and followed by the presentation of a differentiation filter designed within the proposed guidelines.

Step 3: Design of Highpass Filters

Since the frequencies where the long period errors dominate in digitized data represent a small fraction of the whole frequency band of

the data, this becomes the problem of narrow band filtering or of narrow band rejection. An efficient algorithm for the design of narrow band filtering involving multi-stage decimation and interpolation is adopted. The procedure for decimation and interpolation of data involving the design and use of appropriate lowpass filters is also discussed.

Step 4: Automatic Determination of the Frequency band of the Data with Acceptable Signal-to-Noise- Ratio

A frequency band from .07 to 25 Hz has been adopted in routine processing of accelerogram data some ten years ago. However this frequency band actually varies from record to record and sometimes even from component to component, depending upon the signal-to-noise ratio of the data in that range. A subroutine in the data processing software has been developed which, for each input component of the acceleration data, determines the appropriate frequency limits for bandpass filtering in the above steps, so that the resulting data in the band is as free from noise as desireable. This procedure is introduced to control uniformly the signal-to-noise ratio of the data.

Step 5: Design of Integration Filter for the Calculation of Velocity and Displacement Data

With the acceleration data instrument corrected and bandpass filtered, digital integration is performed twice to get the velocity and displacement data. The ideal integration filter is first derived and the problem involved in its implementation examined. The trapezoidal rule of integration originally used together with selected available algorithms are examined and their performances compared. A guideline for the design of the appropriate integration filter is next considered. Criteria for the use of the trapezoidal rule of integration

within the guideline are examined, together with examples of possible new integration filters.

Step 6: Updating Volume III Data Processing

Efficient algorithm for the calculation of the displacement and velocity of the response of a single-degree-of-freedom-system oscillator to earthquake excitation has been used in the calculation of Response and Fourier Spectra for specified natural periods and dampings (Volume III data). The new algorithm results in a saving of as much as 56% of computer time at each step of the iteration.

Step 7: Conclusions - Batch Mode Automatic Digitization and Data Processing

With the automatic determination of the limit frequencies for bandpass filtering, followed by the use of appropriate filters for subsequent bandpass filtering, instrument correction and integration as described above, the batch mode processing for the Volume II stage will now be possible. The existing Volume I processing stage can also be upgraded to make Volume I batch mode processing possible. Currently, Volume III processing is already in batch mode form. This will allow for one batch mode for all Volume I, II and III processing. Together with the Automatic Routine Digitization System completed and operating at USC, this entire package provides an efficient prototype for digitization and data processing of strong motion accelerograms.

CHAPTER II
DIGITAL LOWPASS FILTERS

2.1 Introduction

The aim of this chapter is to explore the availability, characteristics and efficiency of digital filters for low-, high- and bandpass filtering of data in Earthquake Engineering. These are filters whose amplitude response is unity within the passband and zero elsewhere. The passbands for low-, high- and bandpass filters are as shown in Fig. 2.1.1. The frequencies ω_L and ω_H are called cutoff frequencies. The response functions in the figure are those of ideal filters, and will have to be approximated in practice. The three filters will be considered separately. However, most of the attention and discussion will focus on lowpass filters, since these provide the essential relations for deriving either of the other two types.

2.2 Lowpass Filter: Ideal Unit Impulse Response Function

An ideal lowpass filter in the frequency domain passes all low frequencies, $|\omega| \leq \omega_L$, without any change and blocks all high frequencies, $|\omega| > \omega_L$, as given by:

$$H(\omega) = \begin{cases} 1 & |\omega| \leq \omega_L \\ 0 & |\omega| > \omega_L \end{cases} \qquad (2.2.1)$$

The unit impulse response, $h(t)$, and $H(\omega)$ form a Fourier Transform pair, so that:

$$h(t) = \frac{1}{2\pi} \int_{-\omega_L}^{\omega_L} H(\omega)\, e^{i\omega t} d\omega = \frac{\omega_L}{\pi} \frac{\sin \omega_L t}{\omega_L t} \qquad (2.2.2)$$

For an arbitrary time function, $x(t)$, acting as the filter input, the output time function, $y(t)$, is given by the convolution integral of

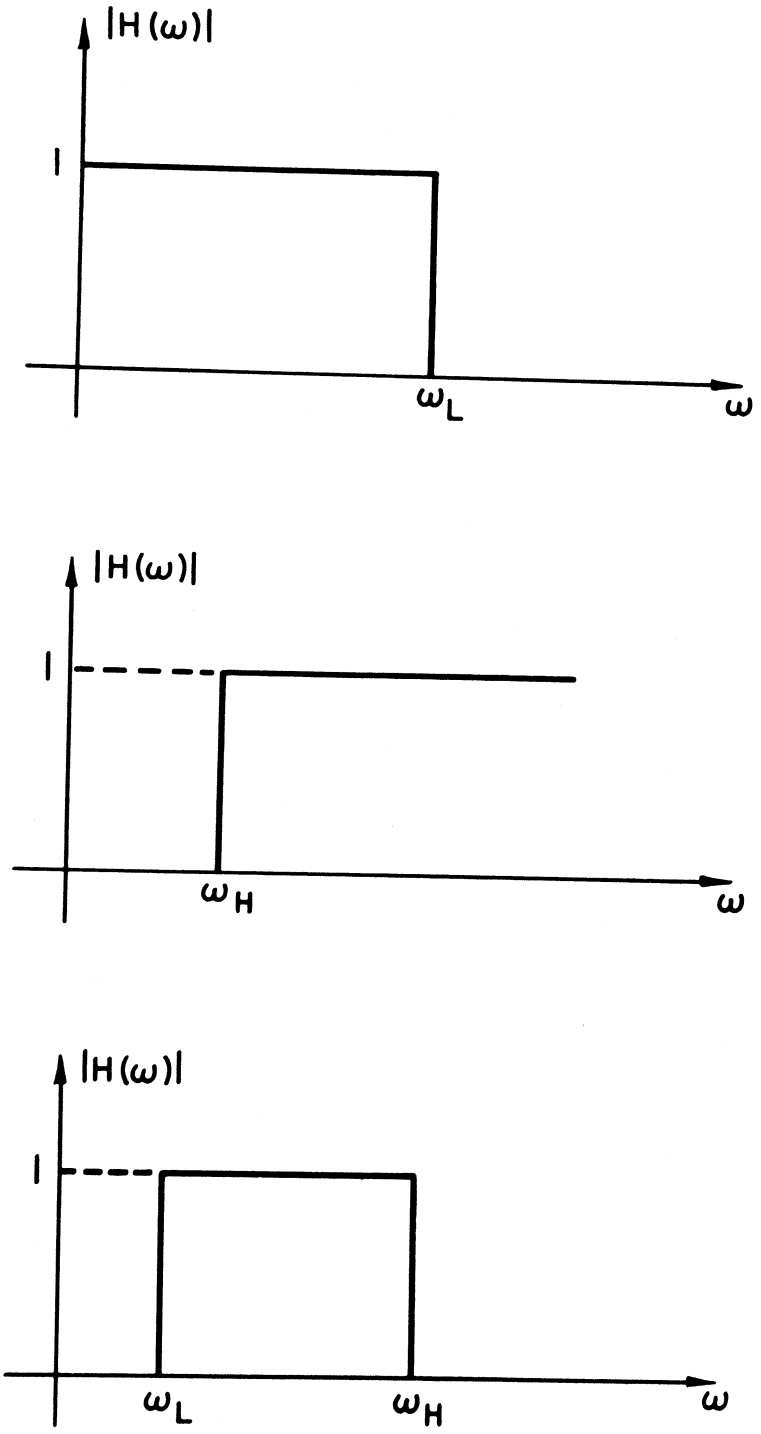

Figure 2.1.1. Ideal low-pass (top), high-pass (center) and band-pass (bottom) filters.

x(t) with h(t),

$$y(t) = \int_{-\infty}^{\infty} h(\tau)x(t-\tau)d\tau \ . \qquad (2.2.3)$$

For digital data sampled at equally spaced intervals of T seconds, the Nyquist (folding) frequency of the input data is given by:

$$\omega_N = \pi/T \ . \qquad (2.2.4)$$

Assume that the cutoff frequency is less than the Nyquist Frequency, $\omega_L < \omega_N$. In the discrete time domain, the ideal lowpass filter can be expressed as complex Fourier Series:

$$H(\omega) = \sum_{-\infty}^{\infty} h[k]e^{-ik\omega T}$$

for $$-\omega_N \leq \omega \leq \omega_N \ , \qquad (2.2.5)$$

and the corresponding impulse-invariant filter weights h[k], are given by:

$$h[k] = \frac{\omega_L T}{\pi} \ \frac{\sin k\omega_L T}{k\omega_L T} \qquad (2.2.6)$$

for k = ...,-2,-1,0,1,2,... from $-\infty$ to ∞. Given the equally spaced set of input data, (x[n]), the output data (y[n]) will then be given by

$$y[n] = \sum_{k} h[k]x[n-k] \qquad (2.2.7)$$

for k = ...,-2,-1,0,1,2,....

An exact realization of an ideal lowpass filter given by (2.2.1) thus requires an infinitely long sequence (h[k]) which extends to infinity in the direction of both positive and negative time.

Several interesting properties of the filter follow directly from (2.2.7). Due to the non-zero values with positive and negative time

indices, it represents a noncausal system. The impulse response sequence (2.2.7) consists of both anticipation ($k < 0$) as well as memory ($k > 0$) terms. Consequently, the output values are influenced by past, present and future input. This requires that the input signal be available in a stored form. For data processing carried out by a computer, this requirement will not create any difficulties.

The impulse response terms (2.2.6) form an even time sequence, with $h[-k]=h[k]$, so that the memory and anticipation (past and future) terms are mirror images of each other. The ideal filter is therefore a symmetric one. Consequently,

$$H(\omega) = h[0] + 2 \sum_{k=1}^{\infty} h[k]\cos(k\omega T) \ , \qquad (2.2.8)$$

so that the transfer function is real. The ideal lowpass filter thus has zero-phase characteristics, and a system described by (2.2.8) will perform a phase-distortionless transmission, a property which is required and essential in most Earthquake Engineering Data Processing applications.

2.3 Truncated Unit-Impulse Response Function With Windowing

A lowpass filter with impulse response function defined by (2.2.7) thus performs an ideal separation of the desired frequency components from the unwanted high frequencies. However, since infinitely long signals cannot be processed by digital computers, the sequence $(h[k])$ has to be truncated. Unfortunately, the convergence of the sequence is slow and large number of terms are needed to get to the sufficiently small coefficients $h[k]$. At the cutoff frequency, ω_L, the transfer function, $H(\omega)$, is discontinuous, changing its value abruptly from 1 to 0.

Taking a finite number of terms in (2.2.8), and substituting the values of h[k] from (2.2.6), will give (Fig. 2.3.1):

$$H(\omega) = h[0] + 2 \sum_{1}^{N} h[k] \cos(k\omega T) \qquad (2.3.1)$$

Truncation will thus introduce errors in the vicinity of the cutoff frequency, a phenomenon known as Gibbs effect. This effect may be reduced by increasing the length of the impulse response. Further, this can be improved by a smoothing technique, known as windowing, in the time domain. Take, for example, Hanning window:

$$w(t) = \frac{1}{2} (1 + \cos \frac{t\pi}{NT}) \ . \qquad (2.3.2)$$

Taking w[t] = w(kT), the "windowed" coefficients become

$$b[k] = h[k]w[k] = \frac{(1 + \cos(k\pi/N))\sin k\omega_L T}{2k\pi} \qquad (2.3.3)$$

and (2.2.7) then becomes

$$y[n] = \sum_{-N}^{N} h[k]w[k]x[n-k] = \sum_{-N}^{N} b[k]x[n-k] \qquad (2.3.4)$$

For example, the transfer function amplitudes for the case of N = 30, $\omega_L = .2\pi/T$, or the cutoff frequency being 1/5 that of the Nyquist frequency, is given in Fig. 2.3.2. Since the filter weights are symmetric, (2.3.4) can be written as

$$y[n] = b[0]x[n] + \sum_{k} b[k](x[n-k] + x[n+k]) \qquad (2.3.5)$$

Another procedure for better and smoother approximations of the discontinuity at the cutoff frequency is to introduce a transition frequency band within which the passband amplitude will gradually

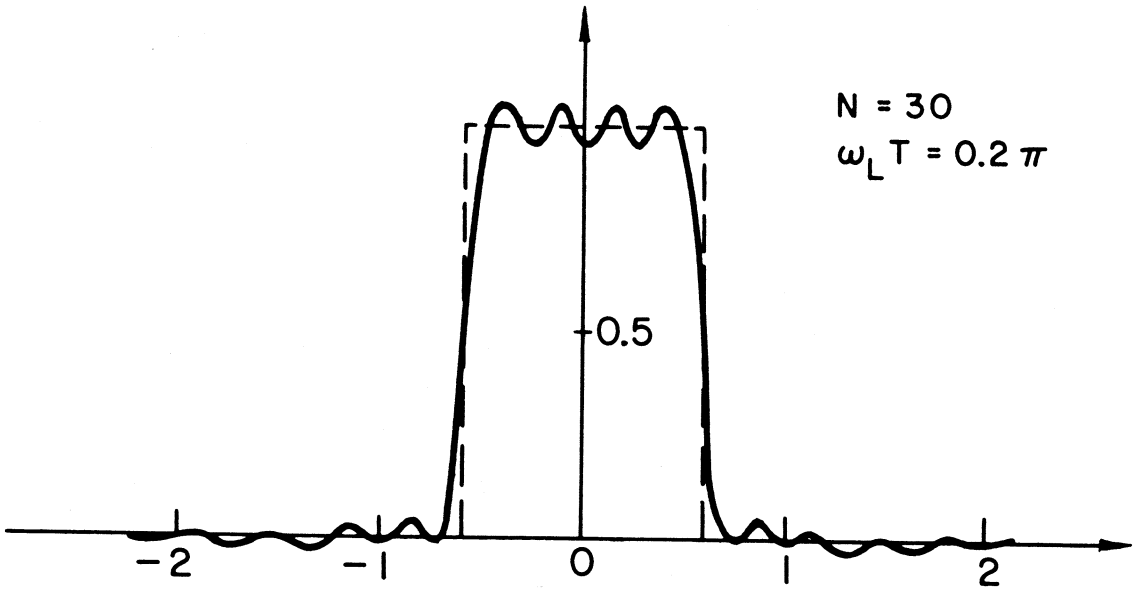

Figure 2.3.1.

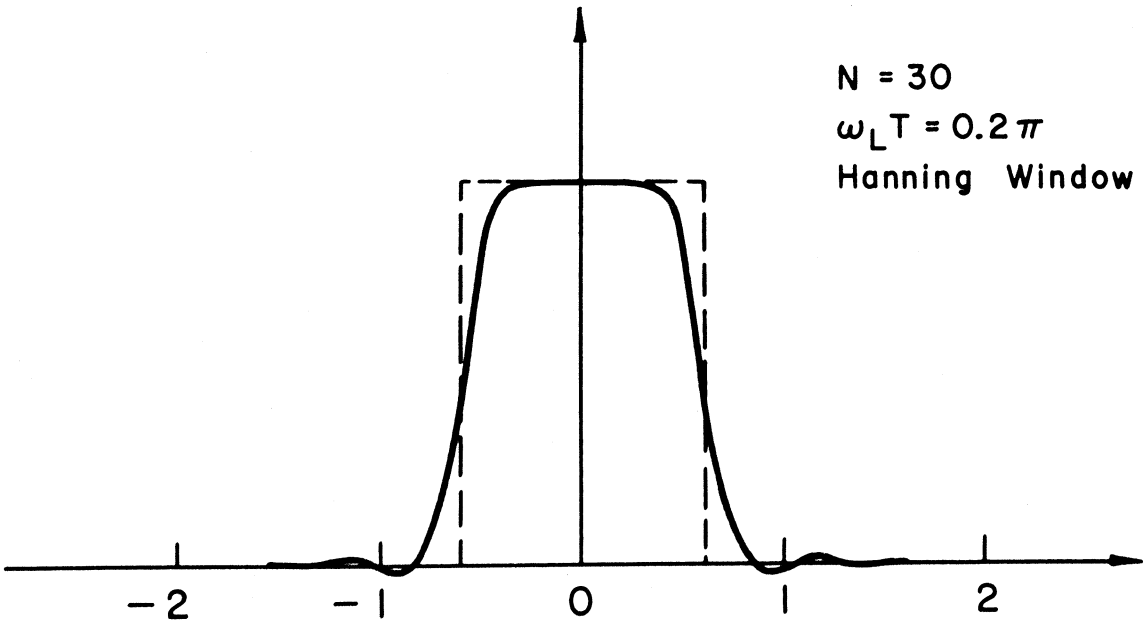

Figure 2.3.2.

Transfer function amplitudes for digital filter with N = 30 and $\omega_L T = 0.2\pi$ (top) and for the same filter with Hanning window (bottom)

decrease or roll off to the stopband amplitude (Fig. 2.4.1). The fine details will depend upon the particular filter design.

A number of methods available for constructing finite-length lowpass filters have been proposed and used for Earthquake Engineering Data Processing. Some of these methods are outlined in the following.

2.4 Ormsby-Type Filter

Anders et al. (1964) proposed the following frequency response function (Fig. 2-4-1) with a first-order roll-off:

$$H(\omega) = \begin{cases} 1 & |\omega| \leq \omega_c \\ 0 & |\omega| > \omega_s \\ (\omega + \omega_s)/\Delta\omega & -\omega_s \leq \omega < -\omega_c \\ (\omega_s - \omega)/\Delta\omega & \omega_c \leq \omega < \omega_s \end{cases} \qquad (2.4.1)$$

where (ω_c, ω_s) is the transition band, $\Delta\omega = \omega_s - \omega_c$. The corresponding impulse response h(t) is given by:

$$h(t) = \frac{\cos \omega_c t - \cos \omega_s t}{2\pi^2 t^2 \Delta\omega} \qquad (2.4.2)$$

The impulse response filter weights for discrete data are again obtained by quantizing h(t) at equal time intervals of kT, for $k\varepsilon(-\infty,\infty)$ giving:

$$h[k] = h(kT) = \frac{\cos \omega_c kT - \cos \omega_s kT}{2\pi^2 k^2 T^2 \Delta\omega} \qquad (2.4.3.)$$

Since the amplitude response $|H(\omega)|$ is now continuous (Fig. 2.4.1), the sequence of weights (h[k]) in (2.4.3) will approximate well the behavior of $H(\omega)$ for sufficiently large k. The filter weights are again symmetric about k = 0, with h(-k) = h(k), so that the filter performs a perfect phase-distoritonless transmission.

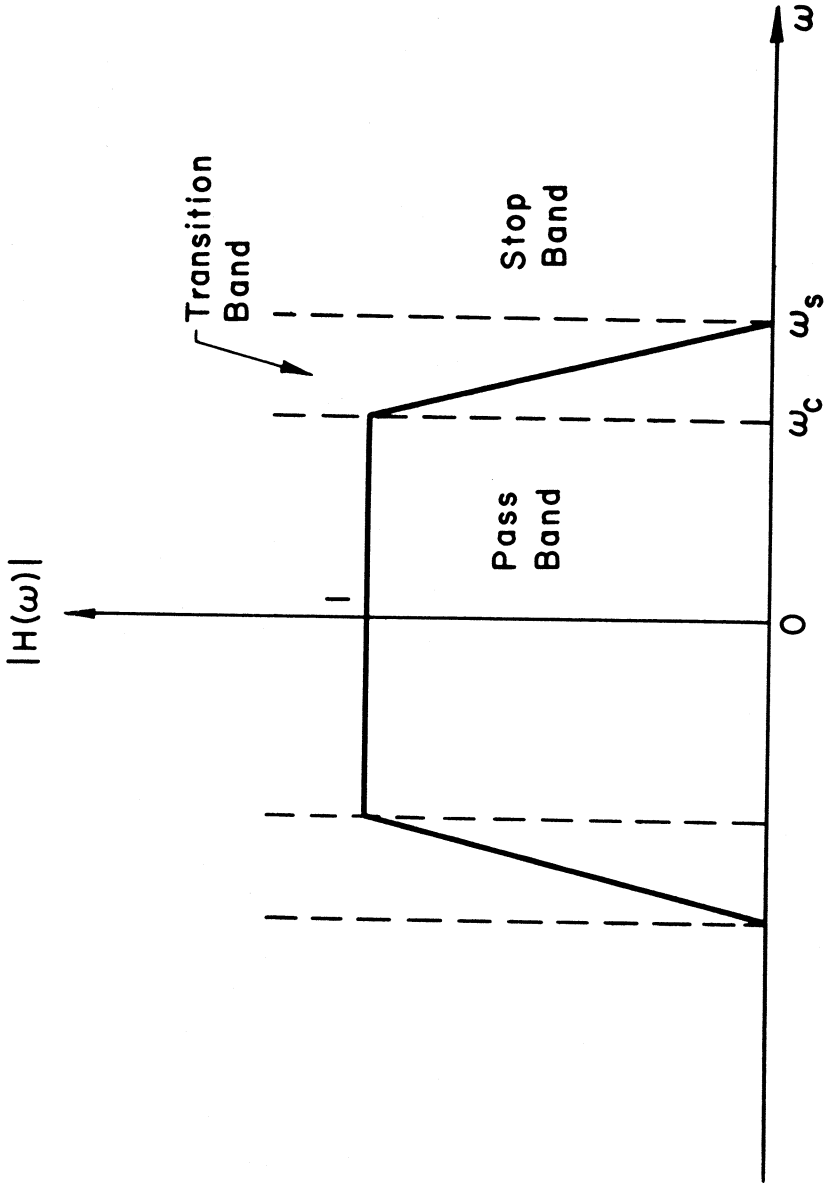

Figure 2.4.1. Low-pass transfer function with transition bands.

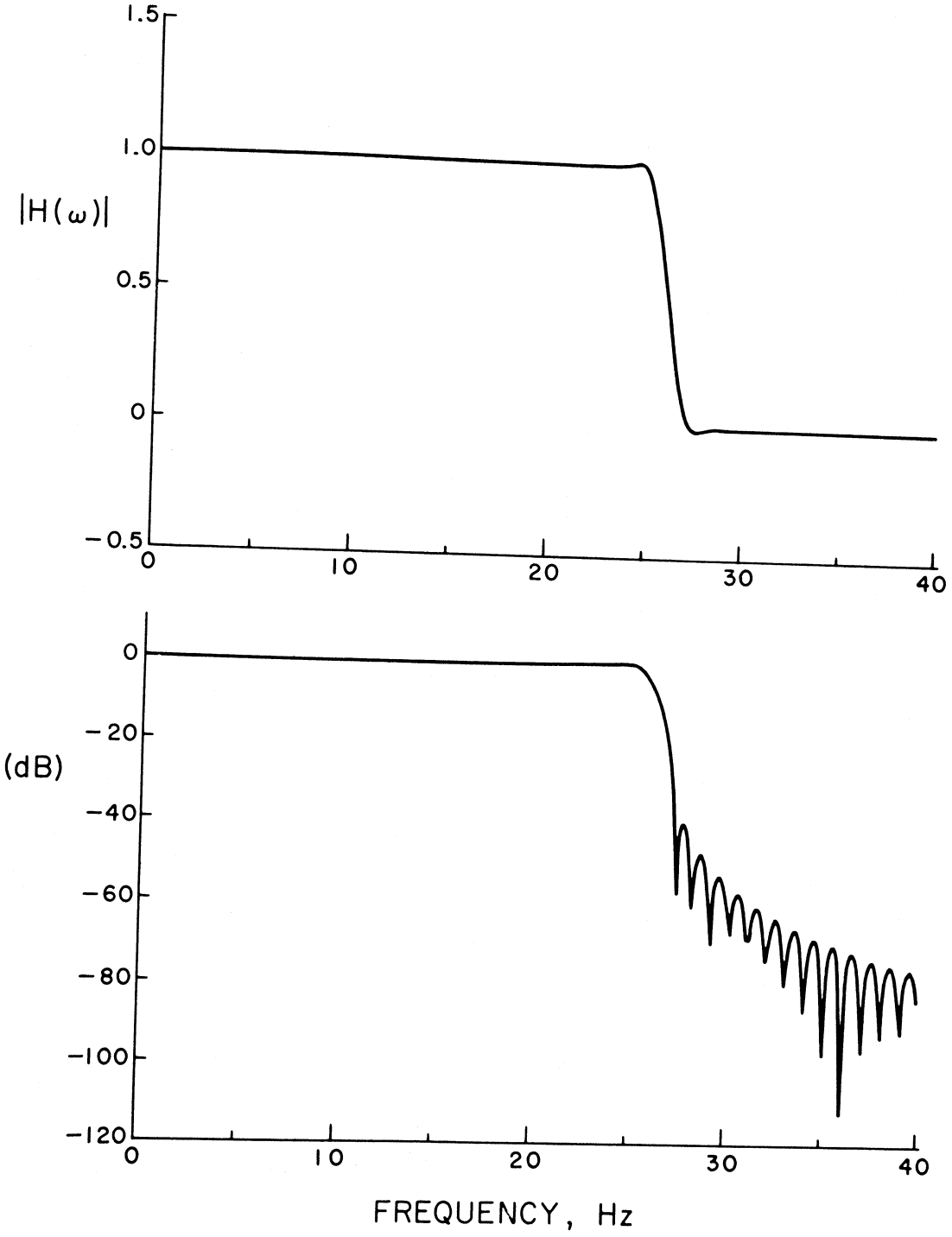

Figure 2.4.2. Ormsby low-pass filter (top: linear amplitude, scale, bottom db amplitude scale).

Fig. 2.4.2 (i) and (ii) show a plot of the truncated Ormsby-type transfer function on linear and logarithmic scales. The cutoff frequency and roll-off frequency interval are 25 and 2 Hz, respectively.

2.5 Chebyshev-(elliptic) Type Filter

Chebyshev (Elliptic) digital filters have been studied in considerable detail (Oppenheim & Schafer, 1975). The design of an elliptic filter involves the approximation of the desired frequency response amplitude by a rational function of the form:

$$H(\omega) = \frac{\sum_{k} b[k] \exp(-ik\omega T)}{1 + \sum_{k} a[k] \exp(-ik\omega T)} \qquad (2.5.1)$$

where the summation for b[k]is from k = 0 to K, and that for a[k] is from k = 1 to L, for some given K,L. The coefficients of the rational function are determined by an appropriate set of specifications on the digital filter. In the case of a lowpass filter, this often takes the form of a tolerence scheme, as shown in Fig. 2.5.1. The dashed line region represents the magnitude of the frequency response of a filter that meets the following specifications:

(1) For a given passband cutoff frequency, ω_c, and a stopband cutoff frequency, ω_s, a transition band of nonzero width, $|\omega_s - \omega_c|$, is assumed in which the magnitude response drops continuously from the passband to the stopband.

(2) Within the passband, $|\omega| \leq \omega_c$, the magnitude of the response must approximate unity to within an error of $\pm \varepsilon_1$:

$$1 - \varepsilon_1 \leq H(\omega) \leq 1 + \varepsilon_1 \qquad (2.5.2)$$

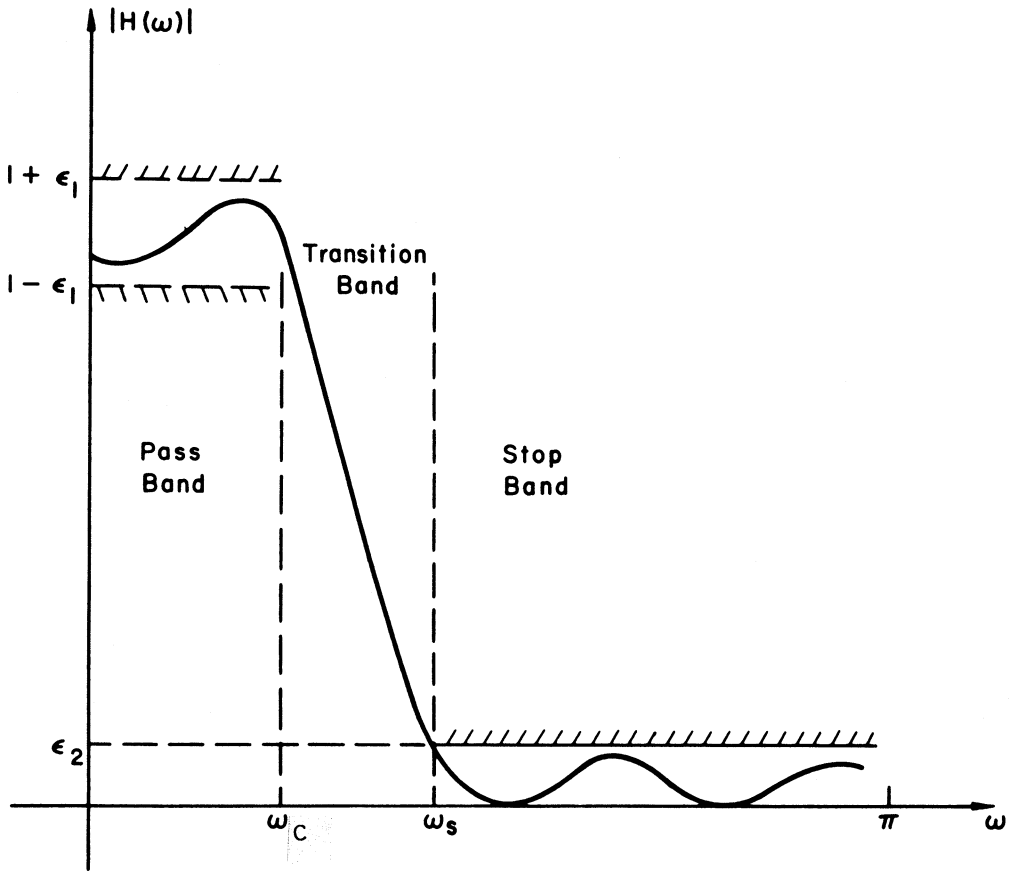

Figure 2.5.1. Tolerance scheme in pass-, transition-, and stop-bands.

(3) Within the stopband, $|\omega| > \omega_s$, the magnitude of the response must approximate zero to within an error of $\pm \varepsilon_2$:

$$|H(\omega)| \leq \varepsilon_2 \tag{2.5.3}$$

For the case of elliptic and other similar filters, like Butterworth filters, there is usually no constraint on the phase response. Often such a filter is determined only in terms of the above magnitude approximation, and the phase of the resulting filter is usually disregarded.

Starting from the equally-spaced input sequence (x[n]), the filter output sequence (y[n]) is given by:

$$y[n] = \sum_k b[k]x[n-k] - \sum_k a[k]y[n-k] \tag{2.5.4}$$

where the summation for b[k]is from k = 0 to K, and that for a[k]is from k = 1 to L.

Note that, in general, the output values are determined in terms of the past and present input plus the past output. A digital filter is completely defined by the sequence (a[k]) and (b[k]), so that designing such a digital filter means finding the constants a[k] and b[k] which will satisfy the given specifications. Elliptic filters are characterized by a magnitude response that is equally rippled in both the passband and the stopband. The frequency response of a lowpass elliptic filter takes the form:

$$H(\omega) = \frac{1.}{1 + \varepsilon^2 U^2(N,\omega)} \tag{2.5.5}$$

where $U(N,\omega)$ is a Jacobian elliptic function. A detailed discussion of the design of such a filter is given in Gold and Radar (1975). The phase $Ph(\omega)$ is given by

$$Ph(\omega) = TAN^{-1}\left(\frac{Imag(H(\omega))}{Real(H(\omega))}\right) \qquad (2.5.6)$$

where Imag(.) and Real(.) are respectively the imaginary and real parts of a complex function. (2.5.1) shows that $Ph(\omega)$ is nonlinear in ω. This means that in general, the filter cannot attain a zero or linear phase characteristics, so that the filter will provide a phase-distorted output. In typical Earthquake Engineering Data Processing, signal distortions due to phase characteristics are not desireable and should be eliminated. To eliminate the phase distortion for a filter of this kind, the original filter may be replaced by the corresponding magnitude-squared filter using a time reversal transformation (Gold & Radar, 1975).

Fig. 2.5.2 (i) and (ii) give a plot of a typical elliptic filter in linear and logarithmic scales, respectively. The passband and stop-band freqeuncies used are 12 to 18 Hz, respectively. Fig. 2.5.3 gives a plot of the phase of the same elliptic filter to illustrate its non-linear characteristics.

2.6 Performance of the Ormsby and Elliptic-type Filters

Comparison of Fig. 2.4.2 (Ormsby) and Fig. 2.5.2 (Elliptic) for the two types of lowpass filters shows similarities in all three bands of frequencies. Both filters approximate unity within the passband, sloping down continuously in the transition band, and within the stopband, the transfer function magnitudes squared are around -40 to -60 dB.

To further compare the performance of the two filters, samples of cosine functions are sampled at 200 points/sec, which is the sampling rate for data currently digitized by the Automatic Digitization Routine System (ARDS) developed at USC (Trifunac and Lee, 1979). For both filters, different frequencies of the input cosine functions from the

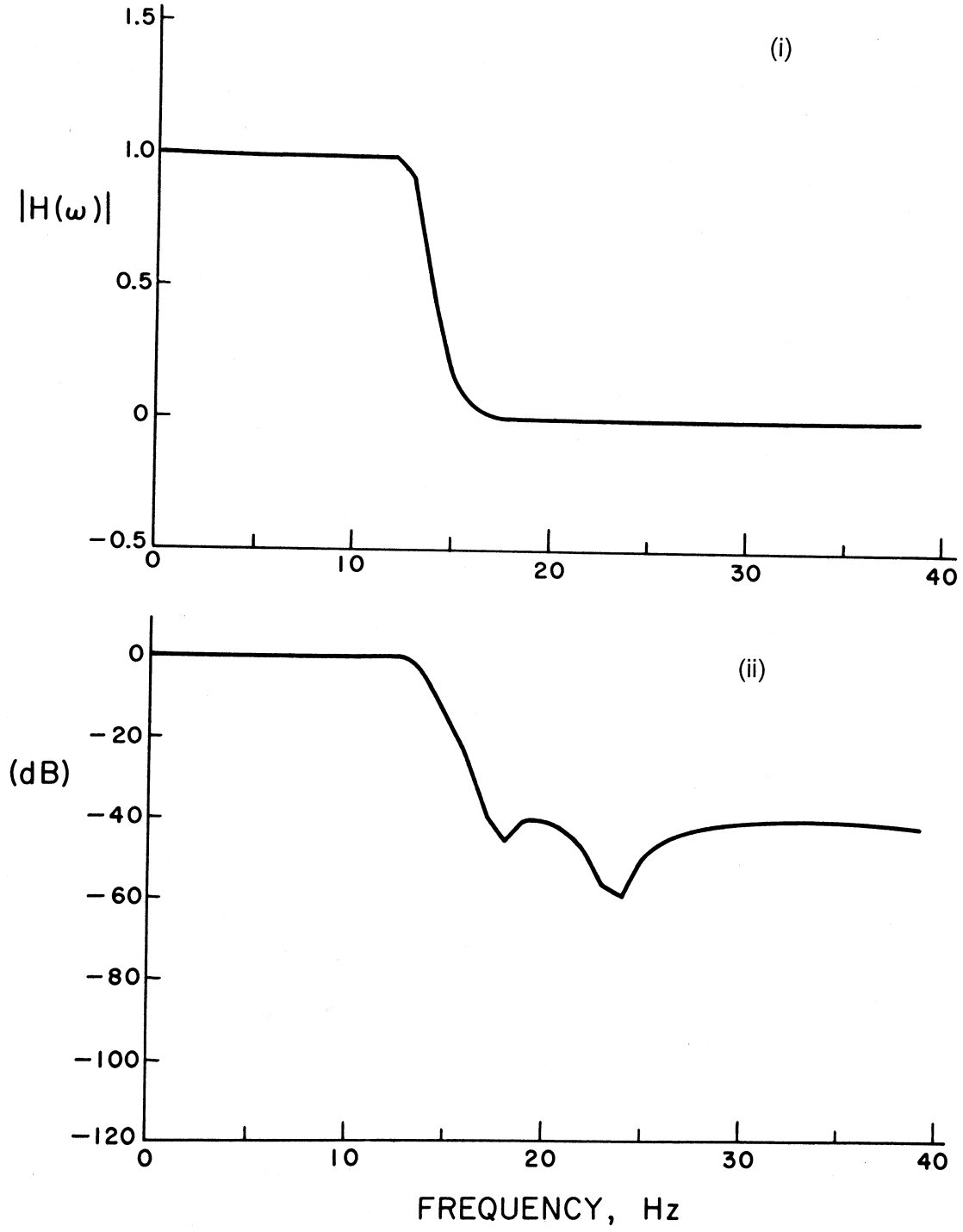

Figure 2.5.2. Elliptic los-pass filter (top: linear amplitude scale, bottom db amplitude scale).

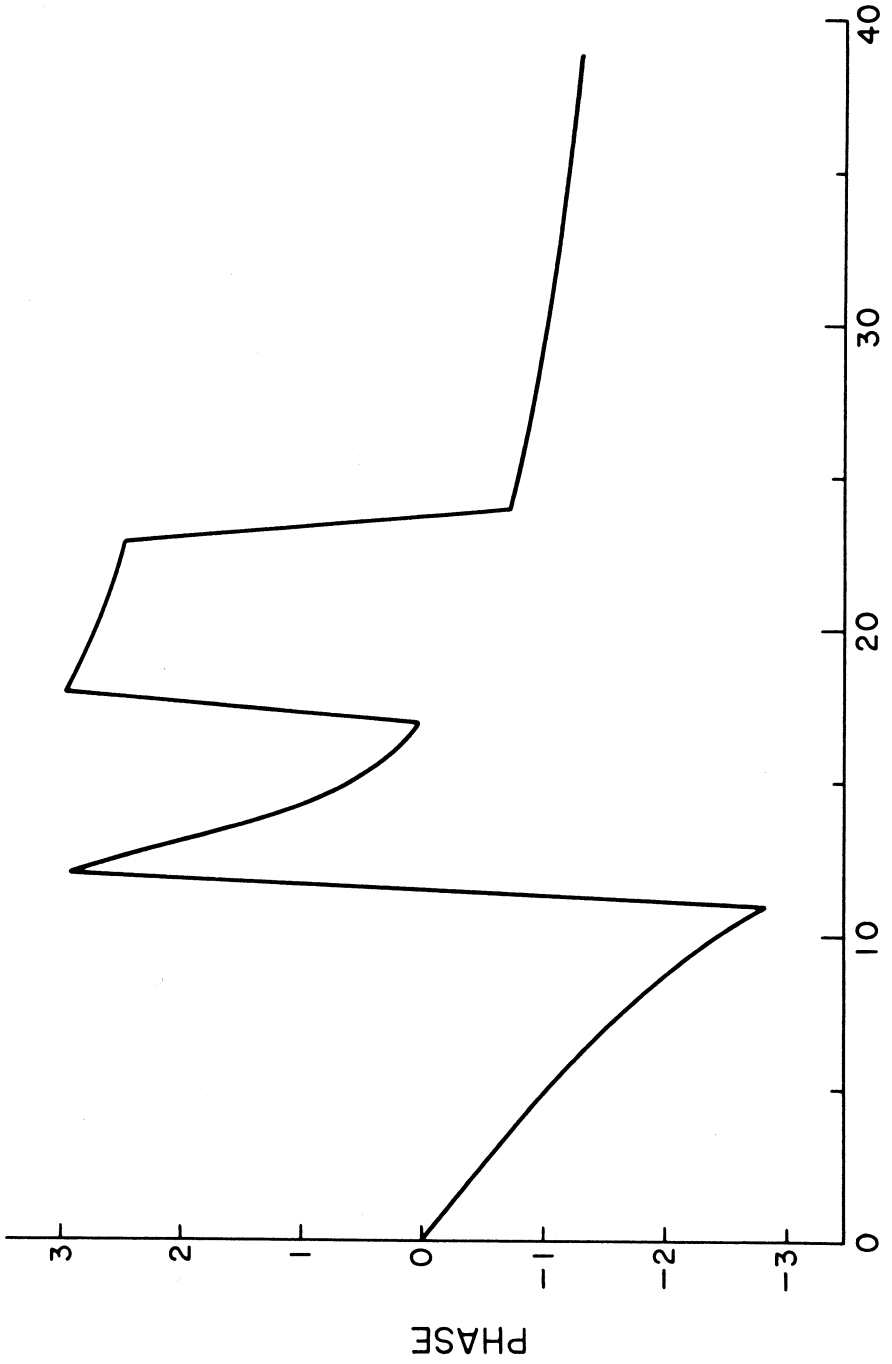

Figure 2.5.3. Phase of the elliptical filter in Figure 2.5.2.

passband through the transition band into the stopband are used. For each frequency, the ratio of the maximum magnitude of the output filtered data to that of the imput data is calculated. This will correspond to the numerical evaluation of the transfer function magnitude of the filter at different frequencies.

Fig. 2.6.1 shows plots of the input cosine functions versus time and the corresponding output functions filtered by the Ormsby filter. The frequencies of input cosine functions in the figure are 8, 16, 24, 28, 32, and 40 Hz. For each plot, the input function is shown by a solid line while the output function is plotted by a dashed line. Since the input functions of different frequencies all have the same sampling rate, the smaller the frequency, the more accurate will the cosine function be represented. The Ormsby filter used has a cutoff frequency of 25 Hz and a transition width of 2 Hz. Thus the first 3 cosine functions of the left in Fig. 2.6.1 are within the passband and hence the corresponding output functions (dashed lines) resemble the imput functions closely in magnitudes and phases. The top function on the right is close to the transition band. The last two functions below are within the stopband and hence the corresponding output functions are approximately equal to zero.

Figure 2.6.2 gives a plot of the input cosine function vs. ωt and the output function filtered by the elliptic infinite impulse response (IIR) filter. Figure 2.6.3 illustrates the use of the IIR filter in the magnitude square sense as described in section 2.5. This means the cosine function is filtered through the IIR filter once, then a time reversal is effected and the result filtered through the IIR filter the second time. The input cosine functions in Figure 2.6.2 and 3 are respectively

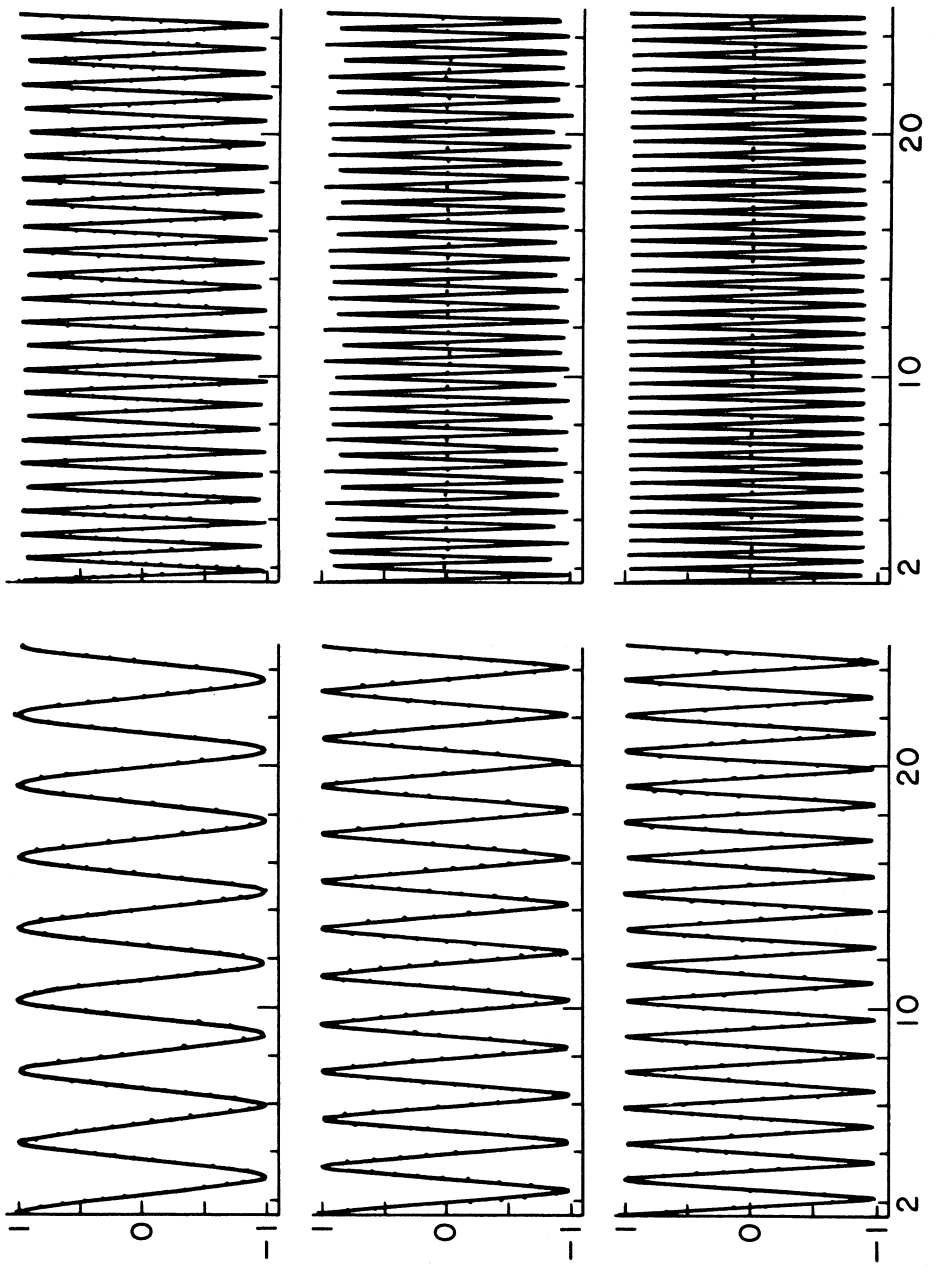

Figure 2.6.1. Input cosine functions (solid line) and output "cosine" functions from Ormsby filter, (dashed line).

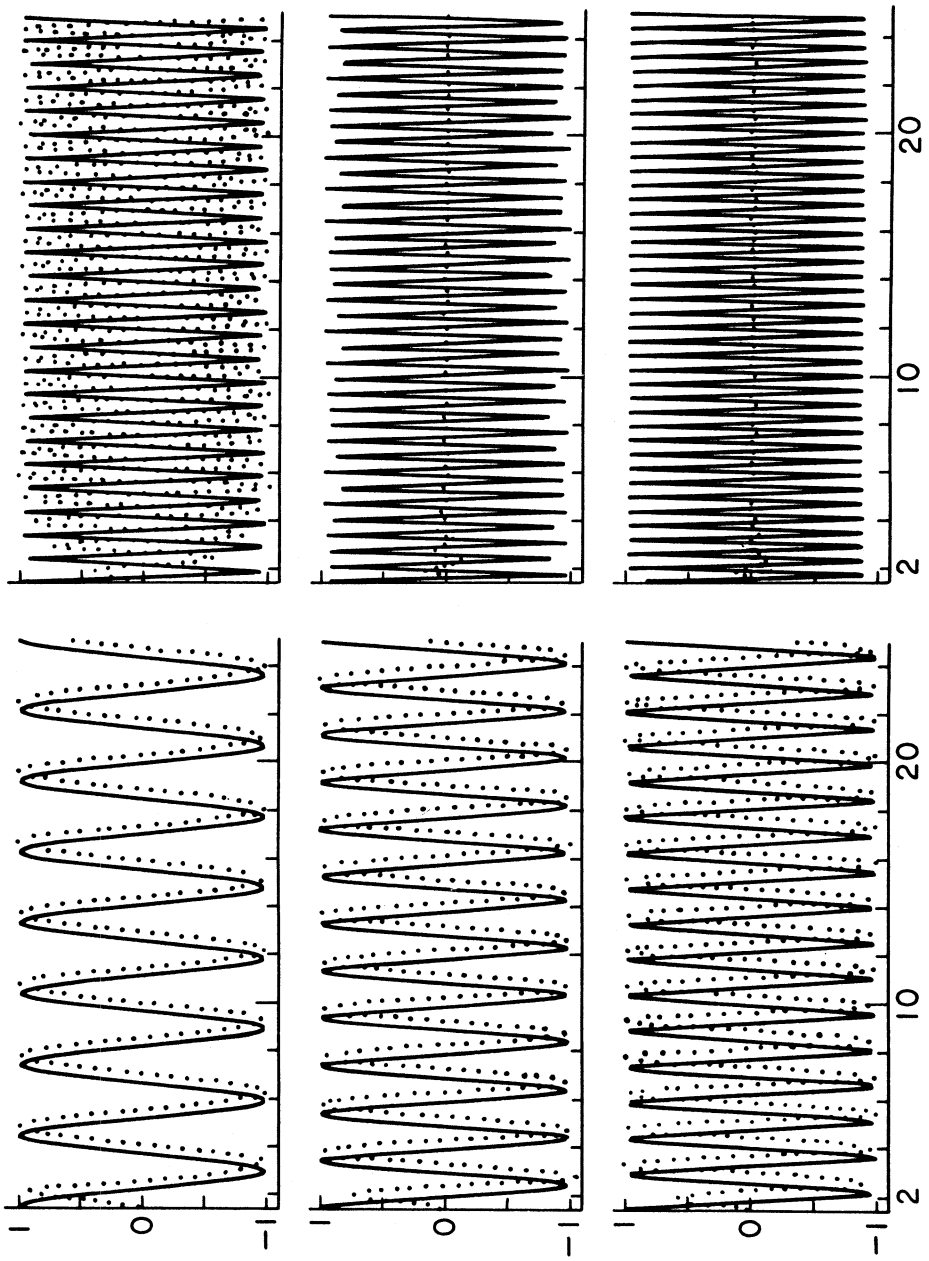

Figure 2.6.2. Input cosine functions (solid line) and output "cosine" functions from elliptic infinite response filter (dashed line).

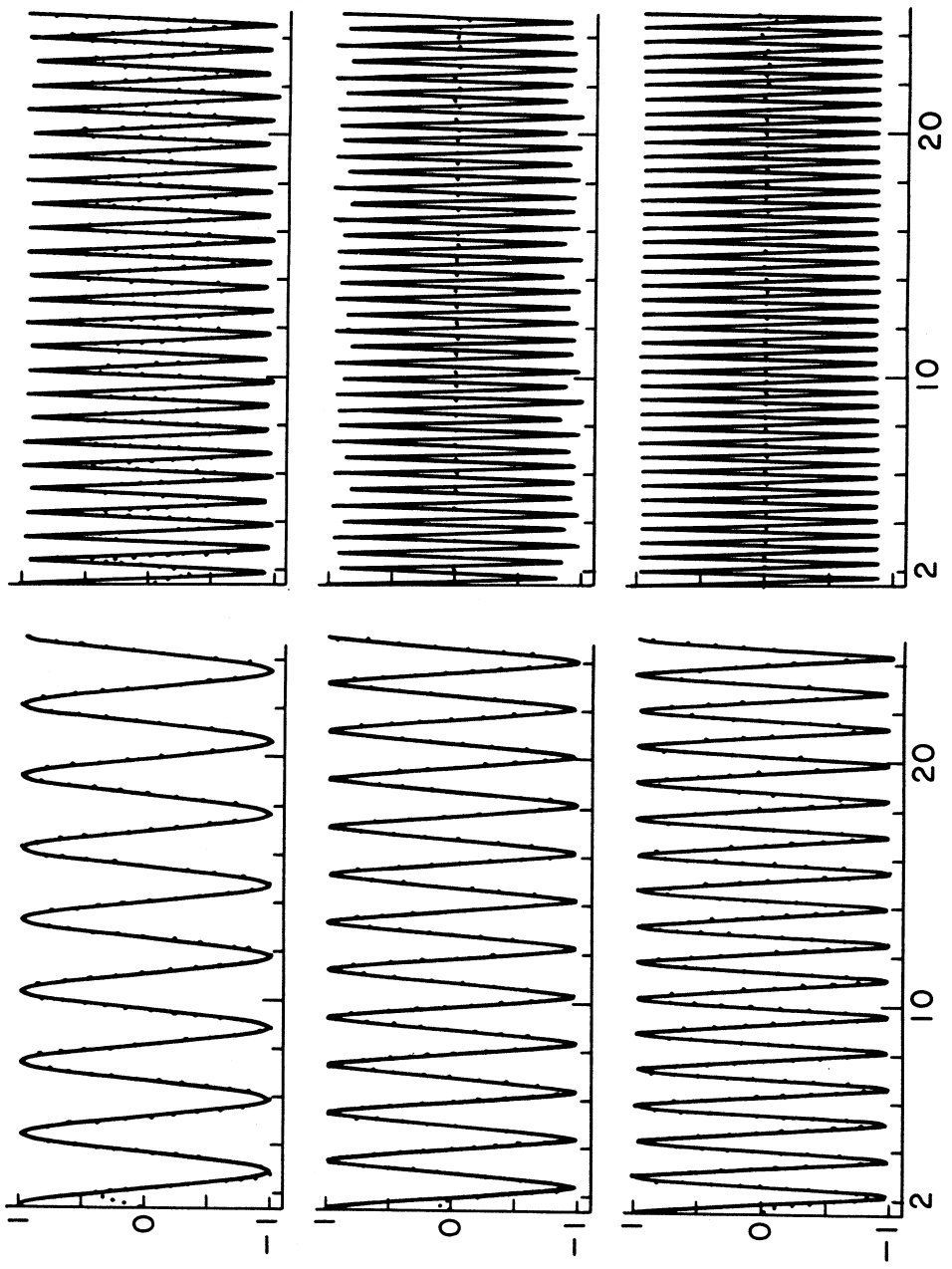

Figure 2.6.3. Input cosine functions (solid line) and output "cosine" functions from elliptic infinite response filter (dashed line) used in the magnitude square sense.

of frequencies 8, 16, 24, 32 and 40 cps as in the example involving the Ormsby filter. For each plot, the solid line again represents the input cosine function and the dashed line the output filtered function. The IIR filter in magnitude squared sense again has a cutoff frequency of 25 cps. The cosine functions on the left half of Figure 2.6.3 are within the passband (respectively 8, 16, and 24 cps). The output functions (dashed lines) resemble the corresponding input functions well except at the beginning where the cosine functions start out with magnitude 1 while the corresponding output functions start out with small magnitude close to 0, and take as much as half a cycle before picking up and being close to the input data. This may be attributed to the fact that the elliptic filter function used only has memory terms and no anticipation terms (Eqn. 2.5.4).

Each point of the output data is determined completely from past and present inputs and past outputs only. At the beginning of time, the outputs are thus determined from and only from little past and present input information. Filters with this causal characteristic are useful when outputs need to be obtained concurrently with inputs.

The Ormsby filter, on the other hand, calculates its outputs from both past, present and future inputs (Section 2.4). In other words, the filter has both anticipation as well as memory terms. This is the reason why the filtered outputs from the Ormsby filter in the passband resemble the inputs almost simultaneously. In earthquake engineering, the input acceleration data are always available in a stored form. Dependence on future inputs thus poses no problem in data processing.

The use of IIR elliptic filter has been suggested by Sunder (Sunder, 1980) because elliptic filters have the unique characteristic of being optimal, in the sense that for a given order and given ripple specifications, no other filter achieves a faster transition between the passband and stopband. However, some optimal filters tend to be robust in their maintenance of performance standards when the given quantities assumed for design purposes are not the same as the quantities encountered in operation. In the case of earthquake engineering, with accelerograms as the input data, signal distortions due to phase characteristics are undesirable and should not be present. Since no phase-distortionless requirement is specified in the design of the IRR elliptic filter, the resulting "optimal" elliptic filter does give a phase-distorted output. To eliminate this, the original filter may be replaced by the corresponding magnitude-squared filter (Section 2.5). The optimality of the resulting filter is thus lost.

2.7 Comparison of the Performance of Ormsby and Elliptic-type filters

With all the input data available in a stored form in a computer before the computation starts, the requirements that the filter be casual (physically realizable) is not essential. This means that the filter used does not have to be recursive, i.e. that the outputs depend only on past and present inputs and past outputs only. (The time reversal step often used with elliptic filter in the correction of phase distortion would have to eliminate this characteristic anyway). In other words, with the input data in stored form, the filter used can have both memory and anticipation terms so that the outputs are dependent on both past, present and future inputs. This results in two important characteristics. First, the impulse response terms (h[k]) can be chosen to form an even time sequence with

$$h[k] = h[-k] \ , \qquad (2.7.1)$$

i.e. with anticipation and memory terms being mirror images of each other. This will result in a filter which will perform a perfect phase-distortionless transmission, an important property in earthquake engineering data processing (Section 2.2).

Secondly, a filter having both memory and anticipation terms as compared to one with just memory terms will mean that it uses more information available about the inputs to produce the outputs. The significance of this is best illustrated in the next two sets of figures. Fig. 2.7.1 shows plots of exponentially decaying input cosine functions versus time and the corresponding output functions filtered by the Ormsby filter. The input data has the same frequencies as those in Fig. 2.6.1, except the amplitudes of the data are now exponentially

decaying, a case which is not uncommon to earthquake data. The output data resulting from the Ormsby filter again resemble the corresponding input data in the passband and have approximately zero amplitudes in the stopband.

Fig. 2.7.2 shows a plot of the numerical evaluation of the transfer function magnitude of the Ormsby filter versus frequency for this particular type of input data. Because of the special transient nature of the input, this may be used to measure the transient character, if any, of the Ormsby filter. The magnitude curve is similar to the case of stationary input already considered (Fig. 2.6.1).

Fig. 2.7.3 shows the same plot of the exponentially decaying input cosine function versus time and the corresponding output data filtered by an elliptic IIR filter. As in the earlier case, the ouptut data all have a phase shift relative to the input data and a correction procedure is again necessary (section 2.6). Figure 2.7.4 shows the same plot of input and output data filtered by the elliptic filter with the time reversal correction procedure. The phase shift is now corrected, but as in the earlier case, the output data again start out with magnitudes close to 0, and take as much as half a cycle before picking up and being close to the input data. The output data thus do not pick up the early and large maxima. Fig. 2.7.5 shows a plot of the numerically calculated transfer function magnitude of the filter versus frequency for this particular type of input data. The transfer function starts out close to unity at low frequency, but then it decreases to .8 at about 5 Hz. It stays at around this magnitude till 20 Hz and then levels to zero at about 30 Hz.

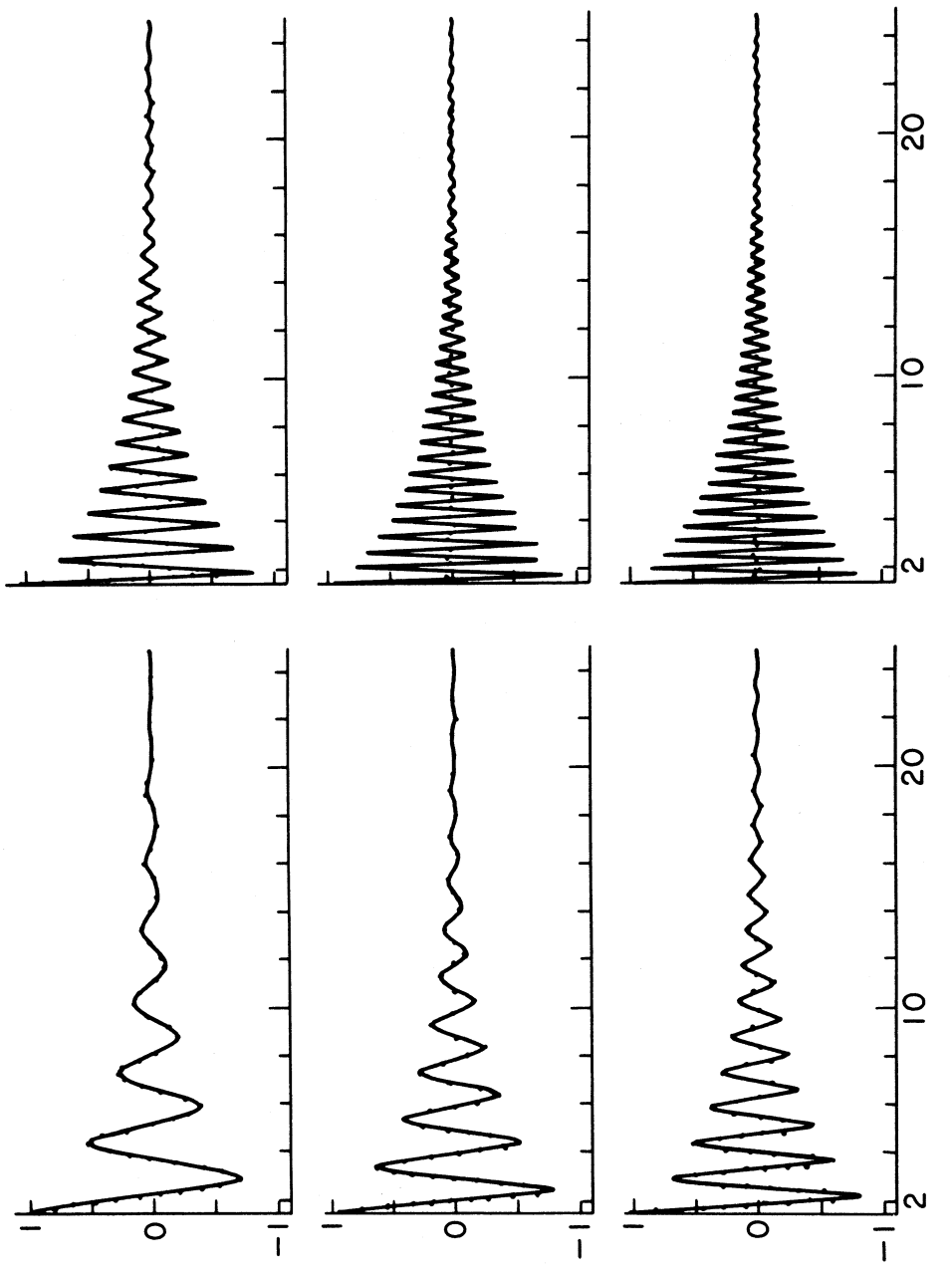

Figure 2.7.1. Input (solid line) and output (dashed line) decaying cosine functions filtered by the Ormsby filter.

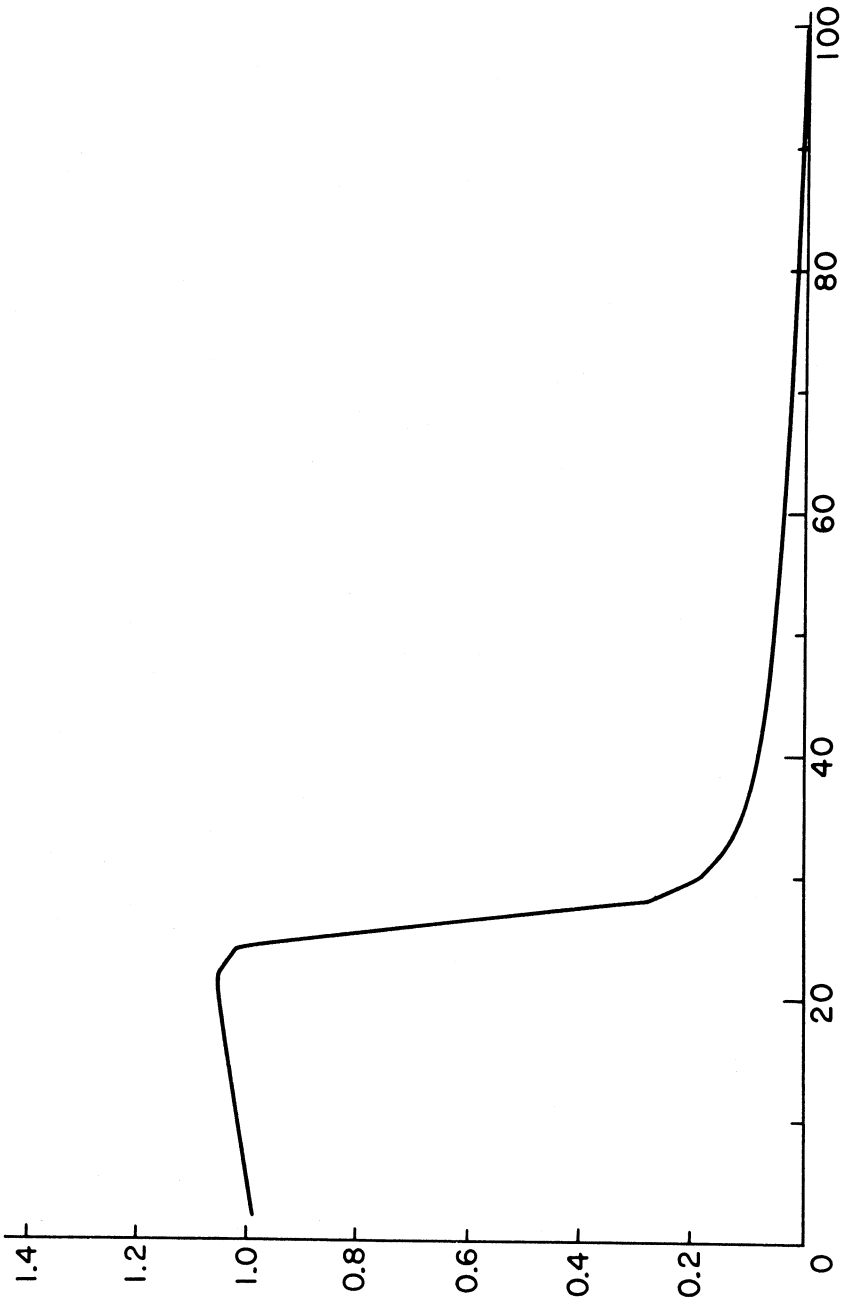

Figure 2.7.2. Transfer function amplitudes of Ormsby filter.

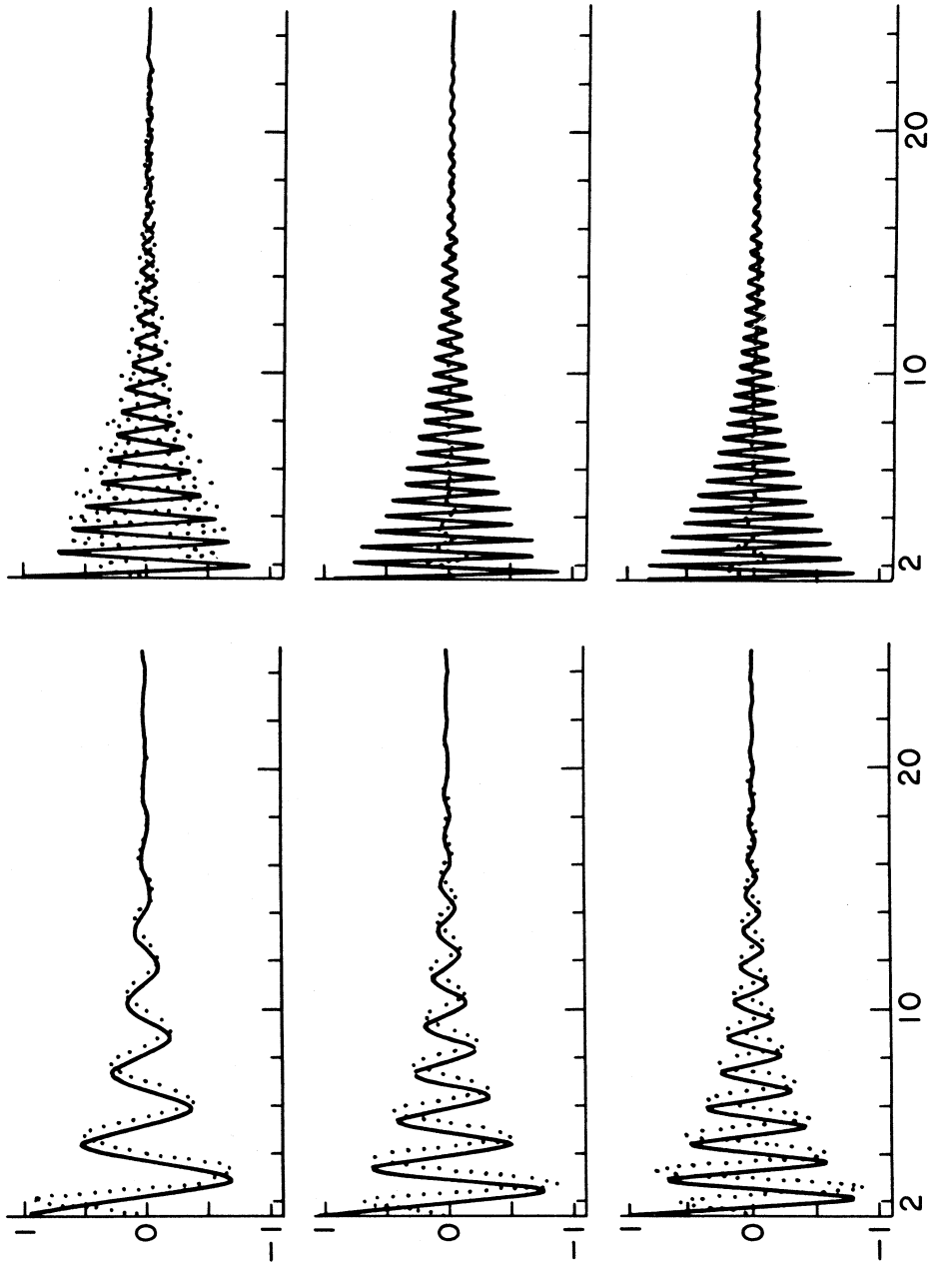

Figure 2.7.3. Input (solid lines) and output (dotted lines) decaying cosine functions filtered by the elliptic IIR filter.

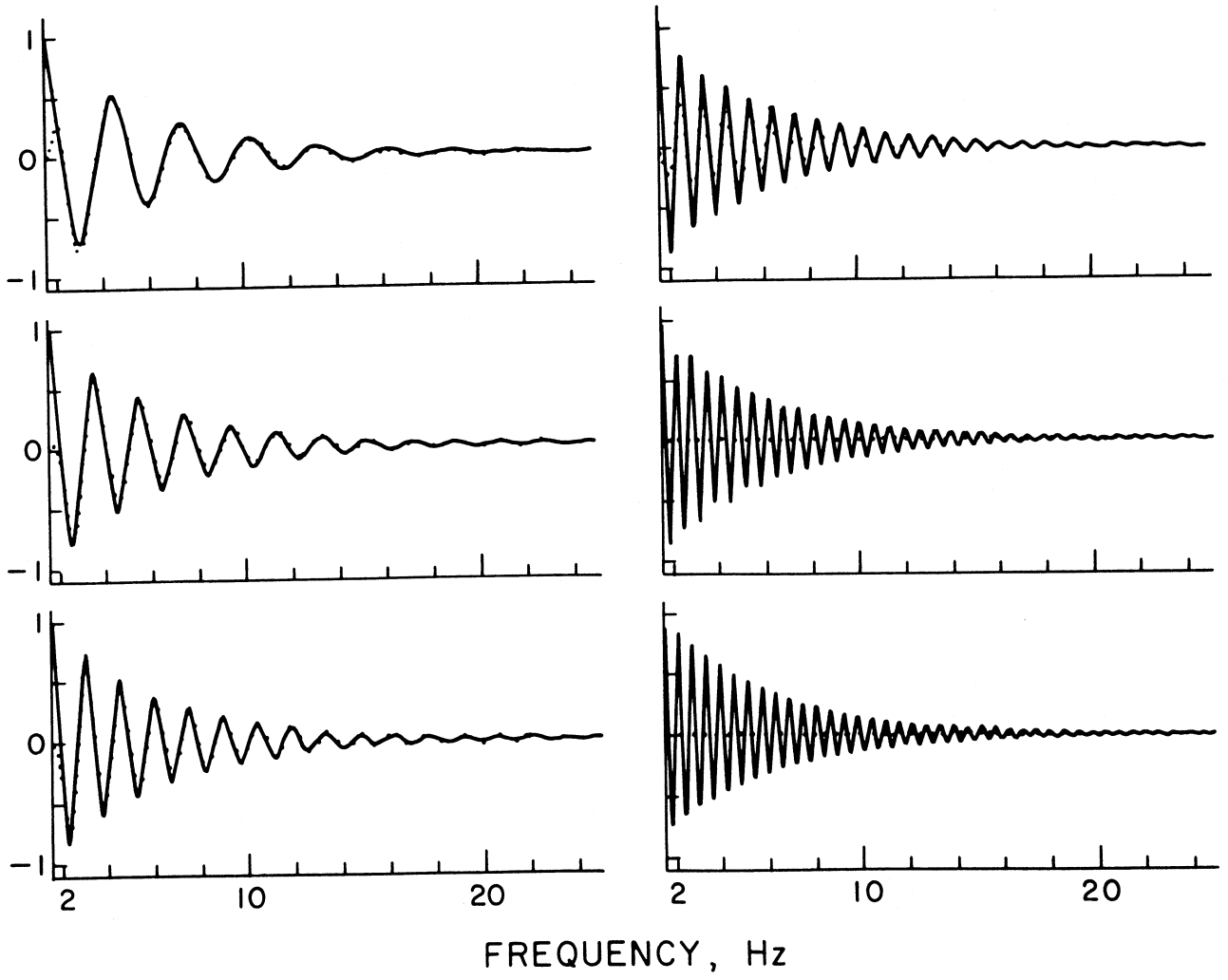

Figure 2.7.4. Input (solid lines) and output (dotted lines) decaying cosine functions filtered by the elliptic IIR filter with the time reversal correction procedure.

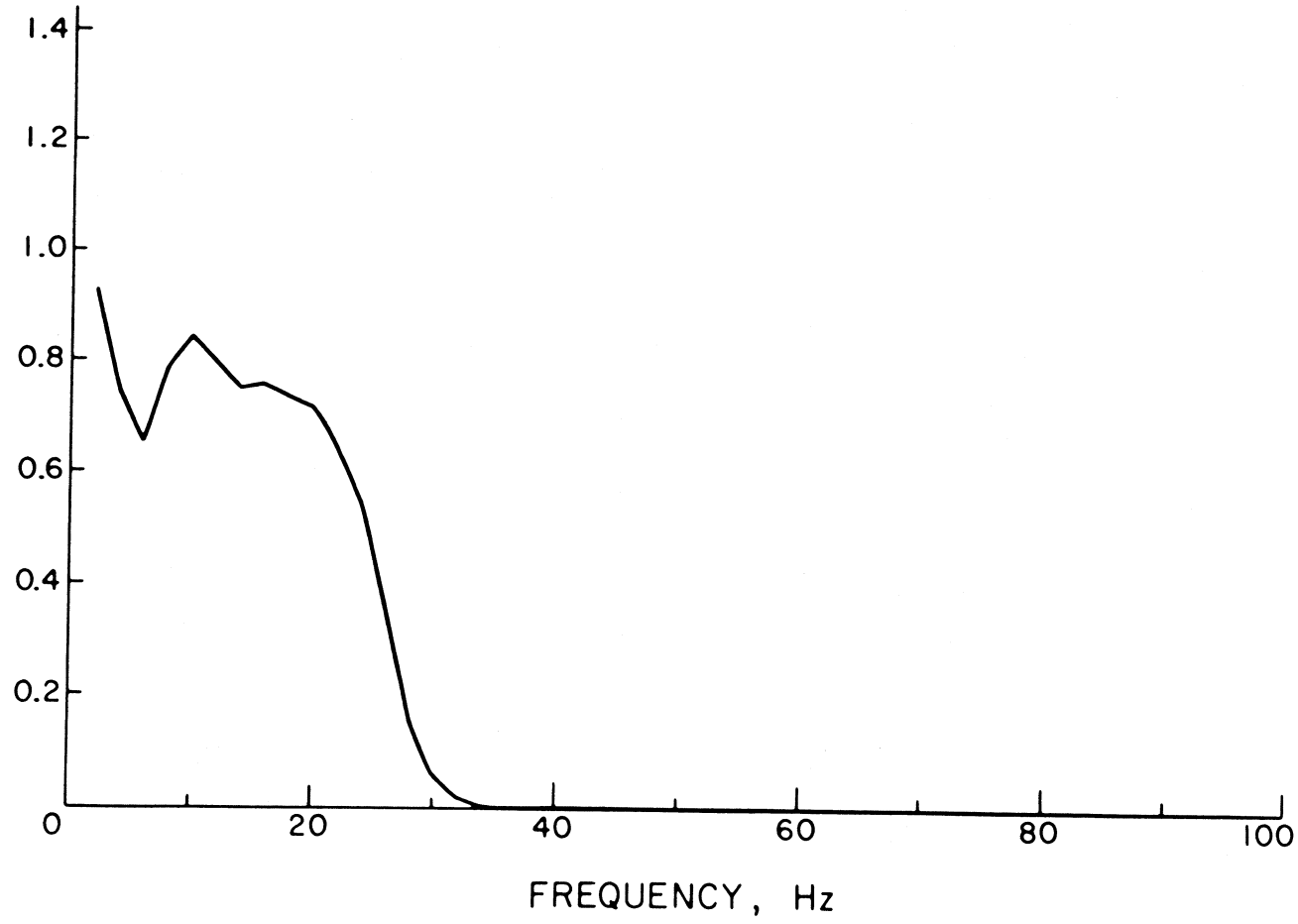

Figure 2.7.5. Transfer function magnitude for data in Figure 2.7.4.

In summary, two types of filters have been considered: Ormsby and Elliptic. The first type performs a perfect phase-distortionless transmission, and with the data in stored form, has both memory as well as anticipation terms. The second type filter gives a phase-distorted output and hence a time reversal technique is needed to correct this. In comparison, both filters show similar performance with constant magnitude cosine functions as input data. However, with decreasing magnitude input cosine function, the Ormsby filter shows a better performance than the elliptic filter.

2.8 Recursive Versus Non-recursive Filters

Two types of filters have been discussed: Ormsby and Elliptic. The first type is a symmetric (h[k] = h[-k]), nonrecursive digital filter which operates on equally spaced data (x[n]) with output (y[n]) given by

$$y[n] = \sum_{k} h[k]x[n-k] \tag{2.8.1}$$

and with a transfer function of the form

$$H(\omega) = h[0] + 2 \sum_{k} h[k]\cos(k\omega T) \ . \tag{2.8.2}$$

The filter performs a perfect phase-distortionless transmission. It has both memory as well as anticipation terms.

The second type is a recursive digital filter operating on equally spaced input data (x(n)) with output (y[n]) given by

$$y[n] = \sum_{k=1}^{L} a[k]y[n-k] + \sum_{k=0}^{K} b[k]x[n-k], \tag{2.8.3}$$

and a transfer function of the form:

$$H(\omega) = \frac{\sum_k b[k]\exp(-ik\omega T)}{1 + \sum_k a[k]\exp(-ik\omega T)} \qquad (2.8.4)$$

a rational function of $\exp(-i\omega T)$. (2.8.4) shows that the filter by itself gives a phase-distorted output and hence a time reversal technique is needed to restore the phase of the input data. It has only memory terms and no anticipation terms.

Comparison of the performance of the two filters is an example of a more general comparison of two types of filters: recursive versus non-recursive filters. The Ormsby filter is a non-recursive filter that, for each n, responds only to values of x[m] in the range (x[n-N],x[n+N]). Non-recursive filters are thus also known as "Finite Impulse Response" (FIR) filters, and elliptic filter used is an example of a "one-sided" physically realizable recursive filter. From its ability to produce, from one single impulse, effects which can extend indefinitely far into the future, it is also known as "Infinite Impulse Response" (IIR) filter.

Both types of filters have about the same flexibility to meet the various conditions. However, a "slow" transient character of the elliptic filter was observed above. At the beginning of time series, it takes time for an elliptic filter to "settle" down after a sudden change in input. The non-recursive Ormsby filter, on the other hand, shows much smaller transient response. Because of such problems, and because of instabilities and phase shifts, recursive filters tend to be used in systems only where there are very long runs of data more or less stationary in character. Non-recursive filters, on the other hand, are simpler to understand, design and use, and are more likely to be used in data processing which are comparatively more transient in nature, as in the case of earthquake engineering data processing, for example.

It is also noted that the elliptic IIR filter has ripples in the transfer function in both the passband and the stopband. Ripples are allowed in its design to achieve its optimality in the order of the filter. Earthquake engineering data processing requires the cascading sequence of many filters, i.e. one filter after another. Bandpass filtering is made of the low- and high-pass filters, instrument correction involves the use of the differentiation filter, twice, to get the first and second order derivatives (Chapter III), integration involves the use of integration and high-pass filters twice to get velocity and displacement data. If the data passes through M such filters with ripple amplitudes $(1 + \varepsilon)$ in the passband, then the resulting ripple peaks will be $(1 + \varepsilon)^M$. Ripples in the passband are thus strongly objectionable in data processing with many cascading filters. Ripples in the stopband are objectionable for the same reason. The input earthquake signal for data processing is often masked by instrument and digitization noise. After filtering out the noise, any small peaks that are left in the spectrum of the signal might result from the original signal or from ripples in the stopband of the transfer functions used in the filtering process. This problem can, and should be, avoided by using a class of filters that vary smoothly throughout their pass-band.

It is with these considerations that the following guidelines are proposed for the design and improvement of new and/or existing low, high and band-pass filters to be used in earthquake engineering data processing:

(1) that the filter be of the form given by (2.8.1), being a finite-impulse response (FIR) non-recursive filter with symmetric coefficients ($h[k] = h([-k])$, so that the transfer function is in the same form

as (2.8.2); this will ensure that the filter performs a perfect phase distortionless transmission;

(2) that the magnitude of the transfer function be free from ripples in both the pass and stop band. The class of filters that vary smoothly should be used;

(3) that the Gibbs effects at the cutoff frequencies due to any form of truncation be minimized; the use of appropriate windowing technique and sharpening technique for smooth transition from the passband to the stopband should be investigated.

2.9 A Note on the Speed of Implementing Non-recursive (FIR) and Recursive (IIR) Filters

For Earthquake Engineering applications, Sunder (1980) suggested the use of recursive (IIR) lowpass filter in place of non-recursive (FIR) filter. He noted that one advantage of the recursive elliptic-type filter over the other filter is in its order, or the number of filter coefficients used. The IIR filter to be used needs to be of an order $K = 5$, and the number of multiplications then equals $N + N + 1 = 11$, and the number of additions 10. Since the correction for phase distortion needs the time reversal technique with the filter applied a second time to the data in reverse order, each point of output thus requires double the number of operations: 22 multiplications and 20 additions.

It was also pointed out by Sunder (1980) that for the realization of Ormsby (non-recursive FIR) lowpass filter, the filter order will have to be as much as 200, or even 500 to satisfy the same design specifications. Each point of the output, according to (2.2.3), would thus need 200 to as much as 500 multiplications. It is often this fact that has made recursive IIR filters thought to be more preferable and efficient when compared to FIR non-recursive filter. However, advances in

signal theory have resulted in the availability of efficient algorithms for the implementation and use of FIR filters. When compared to the use of IIR filters, this results in even greater saving in computation and speed.

The general formula for the application of such a filter is, from (2.3.2):

$$y[n] = \sum_{k=-K}^{K} b[k]x[n-k] \ , \qquad (2.9.1)$$

for n = 1,2,...,N. (2.9.1) is the equation for the discrete linear convolution of (b[k]) and (x[k]). In terms of discrete Fourier Transform (DFT), this becomes:

$$Y(m) = B(m)X(m) \ , \qquad (2.9.2)$$

where B(m), X(m) and Y(m) are respectively the DFT of (b[k]), (x[k]) and (y[k]). High speed Fast Fourier Transform (FFT) algorithm can thus be implemented. Since the input data (x[n]) is often much longer than the filter weights (b[k]), direct implementation of FFT will still not be very efficient. Two new techniques are now available, which both section the long sequence into subsequences and perform partial convolution by the FFT techniques and recombine the results properly to form the desired output sequence.

The first technique is called the OVERLAP-AND-SAVE method. The given shorter sequence (h[k]) is to perform the linear convolution with a comparatively much longer sequence (x[n]). The longer sequence will be sectioned into shorter subsequences and the desired convolution will be achieved through high-speed convolution of the subsequences with the h[k]'s. The procedure is as follows:

(1) Select $L \geq K$, where K is the number of terms in (h[k]) and $L = 2^{**}\ell$ is a power of 2.

(2) Pad the shorter sequence with L - K zeros at the end to make up one of length L.

(3) Form the data sequence $x_i[k]$ having L samples, the first K - 1 of which are to overlap with the preceding segment, i.e. they are simply the last K - 1 samples of the preceding segment. Note that this means that the first segment will be padded with K - 1 zeros at the start for the case of zero extension.

(4) Compute the linear convolution of h[k] with the segment of x[k], both of length L, using the FFT algorithm:

$$y_i[k] = x_i[k] \circledast h[k] \qquad (2.9.3)$$

(5) Discard the first K - 1 samples of $y_i[k]$.

(6) The remaining L - K + 1 samples are then saved and taken as part of the output sequence corresponding to that segment of the x[k] in the linear convolution.

(7) Repeat steps 4 to 6 until all the data are exhausted.

(8) The individual output segments are aligned together to form the overall convolution sequence.

Another method is called the OVERLAP-AND-ADD technique. The procedure is as follows:

(1) Select $L \geq K$, and $L = 2^{**}\ell$, a power of 2, as before.

(2) Pad the shorter h[k] sequence with L - K zeros at the end to make up one of length L.

(3) Form the data subsequences $x_i[k]$ each time by taking L - K + 1 samples from the long sequence x[k] and pad K - 1 zeros at the end to form a segment of length L.

(4) Compute the linear convolution of the two segments of length L, using the FFT algorithm:

$$y_i[k] = x_i[k] \circledast h[k] \tag{2.9.4}$$

(5) The first L - K + 1 samples of this output segment are then placed in the respective positions of the overall output sequence.

(6) The remaining K - 1 samples are to overlap the first K - 1 samples of the subsequent output segment and are added accordingly to the corresponding samples.

(7) Repeat steps (4) to (6) until all data are exhausted.

(8) Combine the segments $y_i[n]$ for $0 \leq n \leq L - K$, as

$$\begin{aligned}
y[n] &= y_1[n] \\
y[n+(L-K+1)] &= y_1[n + (L - K + 1)] + y_2[n] \\
y[n+2(L-K+1)] &= y_2[n + (L - K + 1)] + y_3[n] \\
&\vdots \\
y[n+i(L-K+1)] &= y_i[n + (L - K + 1)] + y_{i+1}[n]
\end{aligned} \tag{2.9.5}$$

Either of the above two techniques is very efficient. Regardless of the method used for combining the partial results, the problem of performing the linear convolution of (2.9.1) has been reduced to performing a series of convolutions of two finite sequences to obtain the partial sequences ($y_i[n]$), that are afterwards suitably combined to obtain (y[n]). To obtain ($y_i[n]$), an L point DFT is first computed on the data segment x[n], to get $X_i[m]$, which is then multiplied term by term with the precalculated (H[m]), the DFT of (h[k]), to get $y_i[m]$,

from which ($y_i[n]$) is obtained as inverse DFT. Using the FFT algorithm, each of the two DFT steps needs L/2*log (L) complex multiplications, and the computation of $Y_i[m]$ takes an additional L multiplications. The total number of multiplications becomes L*(1 + log (L)) for L samples or 1 + log (L) per sample! This corresponds to a drastic savings. As an example, let L = K = 128, then the direct convolution would require 128 multiplications per output sample and the fast convolution needs only 8, that is, a 16 fold reduction. The name fast convolution is thus fully justified. For the case of input samples that are real, further saving of computer time is possible by using FFT algorithms for real data.

2.10 Smooth Nonrecursive Filters

Based on the design criteria set in the previous section, we consider the design of a class of lowpass filters that are monotone (vary smoothly) over the whole frequency band interval. The following approach as described in Hamming (1977) has been adopted.

Given a symmetric (h[k] = h[-k]), nonrecursive digital filter that operates on equally spaced data (x[n]), the output, (y[n]), is computed by the formula:

$$y[n] = \sum_{k} h[k]x[n-k] \ , \qquad (2.10.1)$$

with the corresponding transfer function given by:

$$H(\omega) = h[0] + 2 \sum_{k=1}^{K} h[k]\cos(k\omega) \ . \qquad (2.10.2)$$

Using the identity:

$$\cos(n\omega) = \sum_{k=0}^{n} (-1)^k \, C(n,2k) \cos^{n-2k}(\omega) \, (1-\cos^2(\omega))^k, \quad (2.10.3)$$

(2.10.2) can be transformed into a polynomial in powers of $\cos(\omega)$, which, for suitable choice of coefficients, b[k], takes the form:

$$H(\omega) = \sum_{k=0}^{n} b[k] (\cos(\omega))^k = \sum_{k=0}^{N} b[k] \, t^k \, , \quad (2.10.4)$$

where $t = \cos(\omega)$. As ω goes from 0 to π, t goes from 1 to -1. The original lowpass filter, because of the reversal of the axis in the transform, now appears as a highpass filter in the t variable (Fig. 2.10.1).

Consider the function,

$$g(t) = (1 + t)^p \, (1 - t)^q \, , \quad (2.10.5)$$

with p and q as parameters (Fig. 2.10.1). It has a zero of order p at $t = -1$ and a zero of order q at $t = 1$. Take

$$H(\omega) = \frac{\int_{-1}^{\cos\omega} (1 + t)^p \, (1 - t)^q \, dt}{\int_{-1}^{1} (1 + t)^p \, (1 - t)^q \, dt} \quad (2.10.6)$$

so that, after integration, $H(\omega)$ is a polynomial in $t = \cos\omega$ that has a $(P + 1)$th-order zero at $\omega = \pi$ $(t = -1)$ and the value 1 at $\omega = 0$ $(t = 1)$, along with q derivatives (w.r.t. t) that are zero at $t = 1$. From (2.10.5),

$$g'(t) = 0 \quad \text{when} \quad t = \frac{p - q}{p + q} \quad (2.10.7)$$

which gives the inflection point of the function H(t) in the t domain. Thus, to design a lowpass filter that passes the lower fraction $\alpha, 0 < \alpha < 1$, of the Nyquist interval $(0 < \omega < \pi)$, set

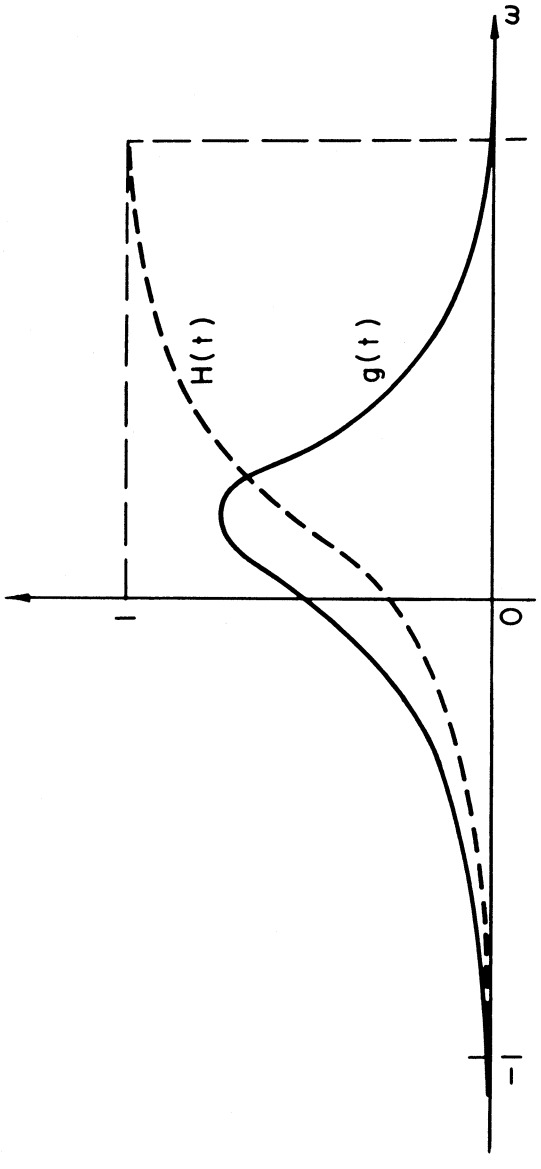

Figure 2.10.1. H(t) (equation 2.10.4) and and g(t) (equation 2.10.5).

$$\frac{p - q}{p + q} = t \simeq \cos\alpha\pi$$

or

$$\frac{p}{q} = \frac{1 + \cos\alpha\pi}{1 - \cos\alpha\pi} \qquad (2.10.8)$$

which gives the ratio of p to q to be used. To get back the h[k] coefficients, the transfer function $H(\omega)$ is transformed back to its Fourier series representation. A detailed description of the procedure is given in Hamming (1962). Fig. 2.10.2 shows the amplitudes, represented by solid lines of these filters versus frequency, ωT, at various cutoff frequencies in the range $0 < \omega T < \pi$. Fig. 2.10.3 shows the same amplitudes in solid lines at logarithmic scale in units of dB. The order of the filters used is around 50. Often in the resulting design of the filter, a big portion of the higher order filter coefficients, h[k], will be virtually so small that they can be taken to be zero. The order of the filter is thus reduced accordingly.

It is seen from Fig. 2.10.2 and 2.10.3 that the resulting filters, as represented by solid lines, all have a fairly wide transition band from 1 to 0. This transition band can be greatly reduced by a sharpening process to obtain a new filter from the old one as given by (Hamming, 1977):

$$H_o(\omega) = H_i^2(\omega) \quad (3 - 2\, H_i(\omega)) \qquad (2.10.9)$$

where

$H_i(\omega)$ is the original filter, and

$H_o(\omega)$ is the new output lowpass filter.

The new filter has the property that the small deviations from unity in the passband and the small deviations from zero in the stopband are

both squared, thus resulting in great sharpening. Thus starting from a program or subroutine that designs the smooth lowpass filter, a new subroutine can be written to:

(a) process the signal once by the lowpass subroutine,

(b) double this output and subtract each output value from 3 times the corresponding input values, and

(c) finally pass this difference through the lowpass filter twice.

This will give a greatly sharpened filter of approximately three times the effective length. Fig. 2.10.2 shows plots of these transfer functions of the smooth lowpass filters. The solid lines are the original filters before they were sharpened by (2.10.9) and the dashed lines give the corresponding sharpened filters. The dashed lines all have a much sharper, narrower transition band than the corresponding solid lines. Fig. 2.10.3 shows the same functions in logarithmic scale. Note that the magnitudes of the data in the stop-band are all < -200 dB.

Compared with the transfer function of the Ormsby filter (Fig. 2.4.2) this filter has a much sharper and narrower transition zone around the cutoff frequency. The Gibbs effect, a result of the truncation of the Fourier series is not present in the smooth filters any more. Windowing is thus not necessary for the smooth filters.

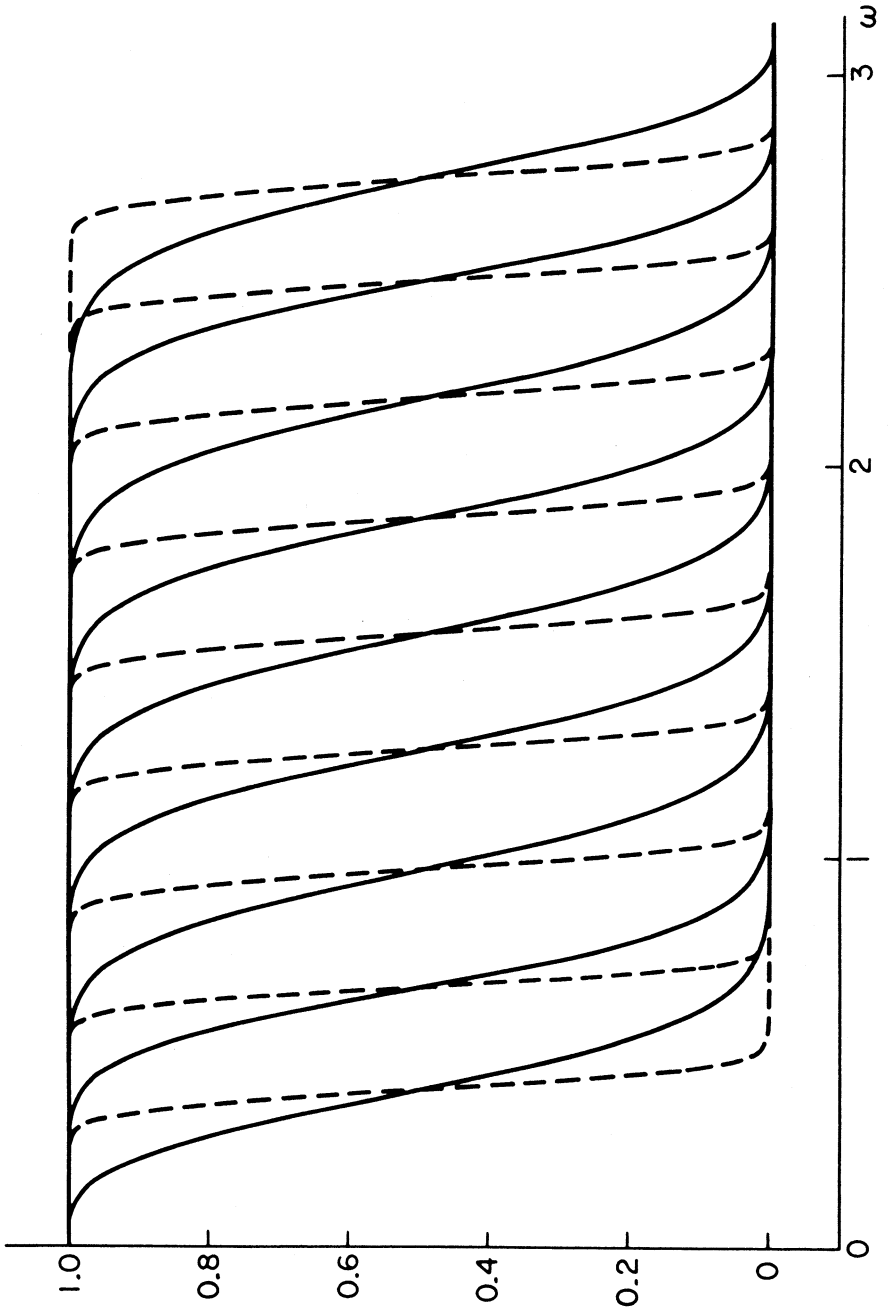

Figure 2.10.2. Smooth low-pass filters (solid lines) and their sharpened transition bands (dashed lines) versus linear amplitude scale.

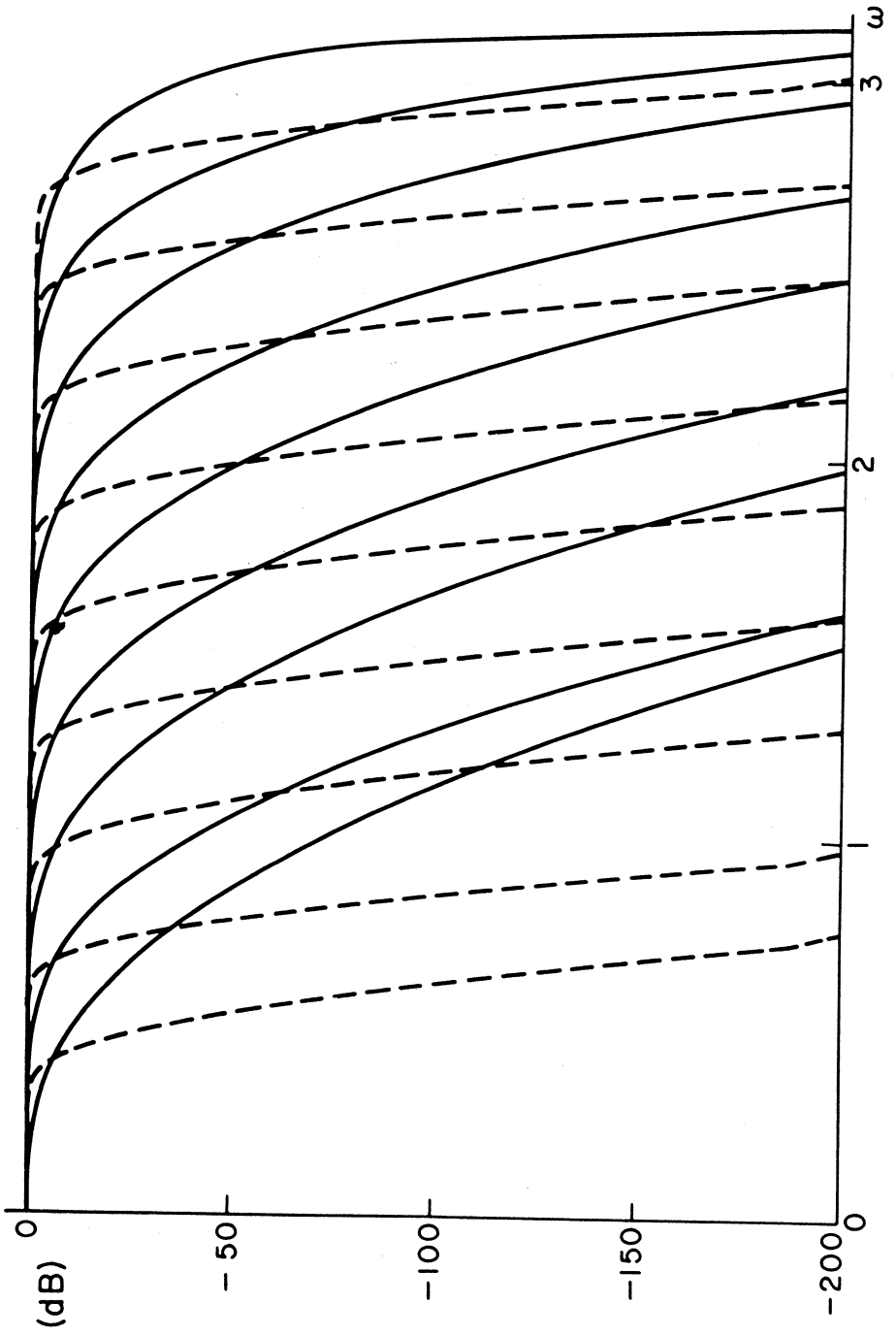

Figure 2.10.3. Smooth low-pass filters (solid lines) and their sharpened transition bands (dashed lines) versus db amplitude scale.

Chapter III

Instrument Correction

3.1 Introduction

The transducer of the recording instrument usually records the relative displacement or relative velocity response of the instrument mass. Instrument correction is then the step that represents the transformation from the transducer relative displacement (or velocity) signal x(t) to the input ground acceleration signal a(t). For example, the dynamic equation of motion of the transducer as a single degree system is given by:

$$\ddot{x} + 2\zeta_o \omega_o \dot{x} + \omega_o^2 x = -a \qquad (3.1.1)$$

where ω_o is the natural frequency of the transfucer, and

ζ_o is the fraction of critical damping.

With the displacement signal x(t) sampled at equally spaced time intervals of T sec. apart, the signal can then be represented as a sequence (x[n]), with

$$x[n] = x(nT) \qquad (3.1.2)$$

for n = 0,1,2,... in the discrete domain. Instrument correction in the discrete domain then leads to numerical differentiation of the sequence (x[n]) once to get ($\dot{x}$[n]) and once more to get ($\ddot{x}$[n]), for use in the equation (from (3.1.1)),

$$a[n] = -(\ddot{x}[n] + 2\zeta_o \omega_o \dot{x}[n] + \omega_o^2 x[n]) \qquad (3.1.3)$$

for n = 0,1,2,... Here (a[n]) represents the sequence of corrected acceleration data in digital form.

With most of the signals x(t) available on analog films recorded by accelerographs, digital data (x[n]) were first obtained by digitizing the record manually. For example, some ten years ago, all of the 1971 San Fernando Earthquake records have been digitized using a Benson-Lahner 099D data reducer unit at California Institute of Technology. These records were then digitized on an unequal time basis, since this would lead to the best definition of the trace for a given number of data points. The average number of digitized points/second was about 20 to 30 in general and up to about 30 to 50 in the most rapidly oscillating sections of the record. The computer software developed for data processing of strong-motion digitized accelerograms (Trifunac and Lee, 1973) interpolated the unequally spaced data to equally spaced data of 100 points/second. The central difference formulae for first and second derivatives. were used:

$$\dot{x}[n] = (x[n+1] - x[n-1])/(2T)$$
$$\ddot{x}[n] = (x[n+1] - 2x[n] + x[n-1])/(T*T) \quad . \qquad (3.1.4)$$

With data at equally spaced time intervals of 0.01 sec. (100 pt/sec) these formulae are accurate up to about 15 Hz, the average sampling frequency of the hand digitized data. No higher order differentiation formulae were thus required nor used for the hand digitized data then. Currently, digital data are available from automatic digitization systems, where, for example, the data are automatically digitized at 200 points/sec. using a Photodensitometer Photoscan P-1000 by Optronics International (Trifunac and Lee, 1979).

3.2 The Differentiating Formulae

It is convenient to examine the numerical differentiating formulae in the frequency domain. This then becomes the problem of designing a filter to estimate the derivative of data given by a discrete sequence. The differentiating filter is to be designed as a linear time-invariant system, where the complex exponential functions $\exp(i\omega t)$ are eigenfunctions. The equation for the derivative:

$$\frac{d}{dt}\left(e^{i\omega t}\right) = i\omega e^{i\omega t} \tag{3.2.1}$$

gives the transfer function of the differentiating filter as (for T = 1):

$$H(\omega) = i\omega \tag{3.2.2}$$

for $-\pi \leq \omega \leq \pi$. The ideal differentiator with cutoff frequency, ω_c, has a transfer function similarly given by:

$$H_D(\omega) = \begin{cases} i\omega & |\omega| < \omega_c \\ 0 & \pi > |\omega| > \omega_c \end{cases} \tag{3.2.3}$$

One general method of filter design is to examine its representation in terms of Fourier series. Writing

$$H(\omega) = \sum h[n] e^{in\omega} \tag{3.2.4}$$

Computing coefficients using the inverse Fourier series formula gives

$$b[k] = \frac{1}{\pi} \int_{-\pi}^{\pi} H(\omega) \sin k\omega \, d\omega = \frac{2}{\pi} \int_{c}^{\omega_c} i\omega \sin k\omega \, d\omega \ ,$$

or

$$b[k] = \frac{2i}{\pi} \left(\frac{\sin k\,\omega_c}{k^2} - \frac{\omega_c \cos k\,\omega_c}{k} \right) \tag{3.2.5}$$

with the cutoff frequency $\omega_c = \pi$, this gives

$$b[k] = \frac{-2i \cos \pi k}{k} = \frac{2i}{k} (-1)^{k+1} \qquad (3.2.6)$$

We thus have an infinitely long sequence that we must truncate. Truncating the Fourier series will lead to Gibbs effect, and windowing is again necessary. Fig. 3.2.1 gives a plot of the transfer function amplitude of (3.2.2) using K = 10 terms of the coefficients given by (3.2.6), which shows the overshoot near the cutoff frequency, ω_c. Fig. 3.2.2 gives a plot of the same function using windowing.

In the design of a digital differentiator, it is seen that for the filter to be purely imaginary, as in (3.2.2) or (3.2.3), the coefficients of the filter must have odd symmetry, that is

$$h[-k] = - h[k] \ , \qquad (3.2.7)$$

for all k, so that

$$h[k](e^{ik\omega} - e^{-ik\omega}) = 2i\, h[k] \sin k\omega \qquad (3.2.8)$$

and the filter has a sine series representation. Thus with x[n] denoting the digital derivative of x[n], the differentiating formula should take the form:

$$\dot{x}[n] = \sum_{-k}^{K} h[k]\, x[n-k] \qquad (3.2.9)$$

with h[0] = 0 and h[-k] = - h[k], which will lead to the sine series

$$H(\omega) = 2i \sum_{1}^{K} h[k] \sin k\omega \ . \qquad (3.2.10)$$

(3.2.9) can be rewritten as

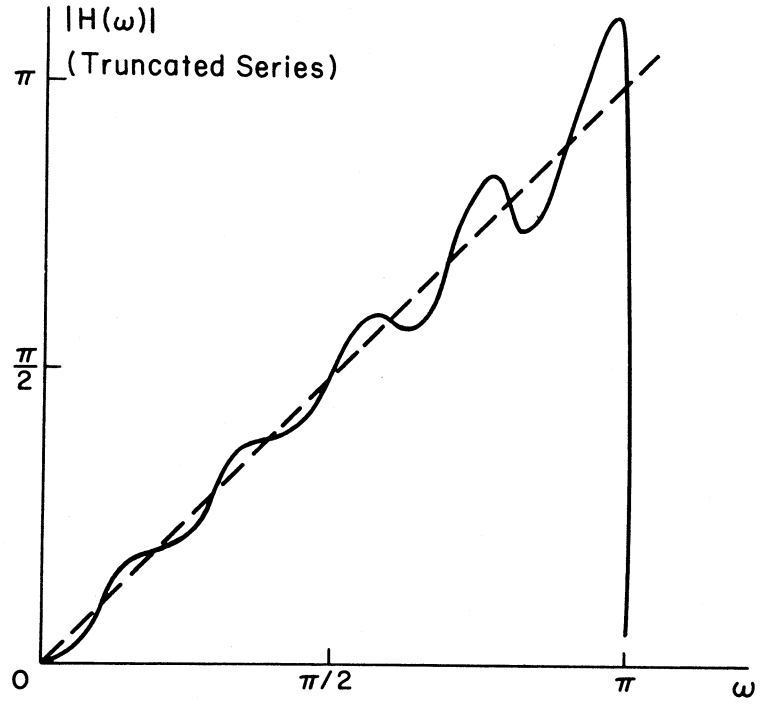

Figure 3.2.1. Transfer function amplitude for K = 10.

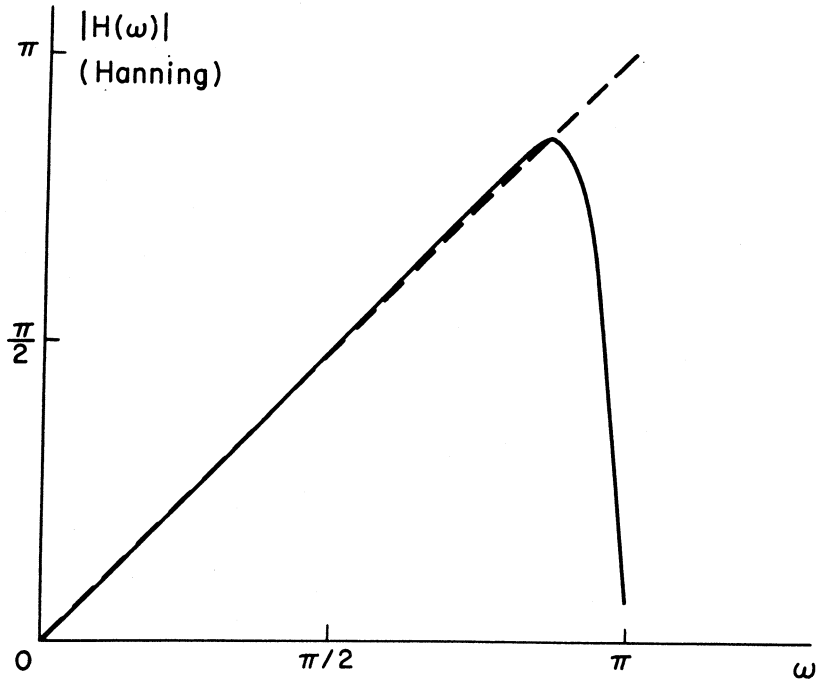

Figure 3.2.2. Transfer function amplitude for K = 10 and Hanning window

$$\dot{x}[n] = \sum_{1}^{K} h[-k]\ (x[n+k]-x[n-k]) \qquad (3.2.11)$$

which is a linear combination of differences of symmetrically placed values of the function. In other words, (3.2.11) can be considered as an n-th order central difference formula, one that will give a transfer function that is purely imaginary as required and can thus be designed to best approximate the ideal differentiator in (3.2.2) or (3.2.3).

3.3 The Classical Differentiating Formulae: Example

The classical 3-points' and 5-points' central difference formulae have transfer functions given by:

$$\begin{aligned} &\text{3 points } (K = 1): && H(\omega) = i \sin\omega T/T \\ &\text{5 points } (K = 3): && H(\omega) = i\ (8\sin\omega T - \sin 2\omega T)/6T \end{aligned} \qquad (3.3.1)$$

With digitized data now available at 200 points/sec, or at time spacing of T = .005 sec, Fig. 3.3.1 shows a plot of the normalized transfer function amplitudes of ($|H(\omega)/\omega|$ in (3.3.1) versus frequencies in Hz. The ideal transfer function will have a normalized amplitude of $|H(\omega)/\omega| = 1$ for all frequencies.

At 25 Hz, the lowpass cutoff frequency currently used in routine data processing (Trifunac and Lee, 1979), the 3-points' formula has a normalized magnitude of .8, while the 5-points' formula has magnitude of .98. Out at 50 Hz, their magnitudes are down to .64 and .98, respectively. Sunder (1980) proposed the use of 9-points' differentiating formulae obtained from the design of a Finite Impulse Response (FIR) filter with ripples. With data he proposed to be sampled at 100 points/sec, or a Nyquist frequency of 50 Hz, their normalized transfer function magnitudes versus frequencies are plotted in Fig. 3.3.2. At

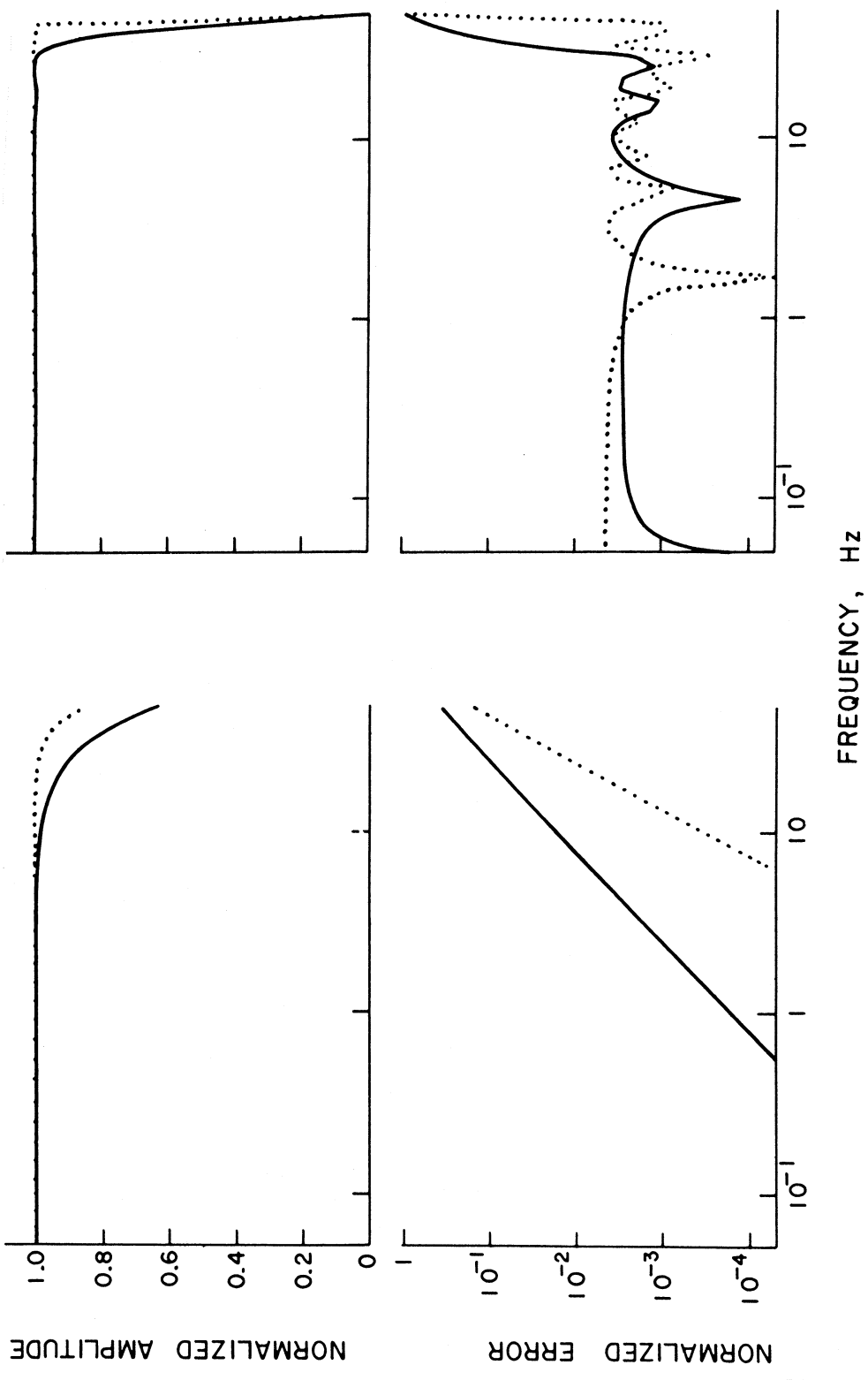

Figure 3.3.1. Three point (solid lines) and 5 point (dotted lines) transfer function $|H(\omega)/\omega|$ versus frequency for $\Delta T = 0.005$.

Figure 3.3.2. Nine point (solid lines) and 31 point (dotted lines) transfer function amplitudes of $|H(\omega)/\omega|$ using FIR and $\Delta T = 0.01$.

25 Hz, both formulae have magnitudes close to 1, while at 50 Hz, the proposed Nyquist frequency, both have magnitudes decreasing rapidly to 0.

The question naturally arises, whether the 9-points or 31-points' FIR differentiating formulas proposed by Sunder (1980) should make any difference, if any, to the instrument correction step performed on the manual digitized data in the last 10 years in routine processing. Fig. 3.3.1 shows a plot of the logarithm of the normalized error amplitudes versus frequencies, where

$$\varepsilon(\omega) = |H(\omega)/i\omega - 1.| \qquad (3.3.2)$$

for the central difference 3-points' and 5-points' formulae. The magnitude of the errors are significantly less than .01 for frequencies up to 10 Hz. Fig. 3.3.2 shows the same error amplitudes for the 9-points' and 31-points' FIR formulae. The magnitudes of the errors are systematically of order around .01 all through the range of frequencies considered. This is the result of allowing ripples in the design of the FIR filter, a fact which has already been discussed in section 2.8.

Fig. 3.3.3 gives a plot of the average Fourier spectra versus period at M.M.I. levels of IV, VI, VIII, X and XII. It is obtained by empirical scaling of 186 strong-motion earthquake records (Trifunac and Lee, 1978). The data are obtained by manual digitization at Caltech for analog records obtained for earthquakes in the years from the 1933 through 1971. The plot shows that the Fourier amplitudes at periods $T < .05$ sec, or at frequqncies $f > 20$ Hz, are less than 10% of the average amplitudes in the whole range of frequencies (.07 to 25 Hz). The previous three figures thus lead us to the conclusion that the different differentiating formulae will not lead to any significant change

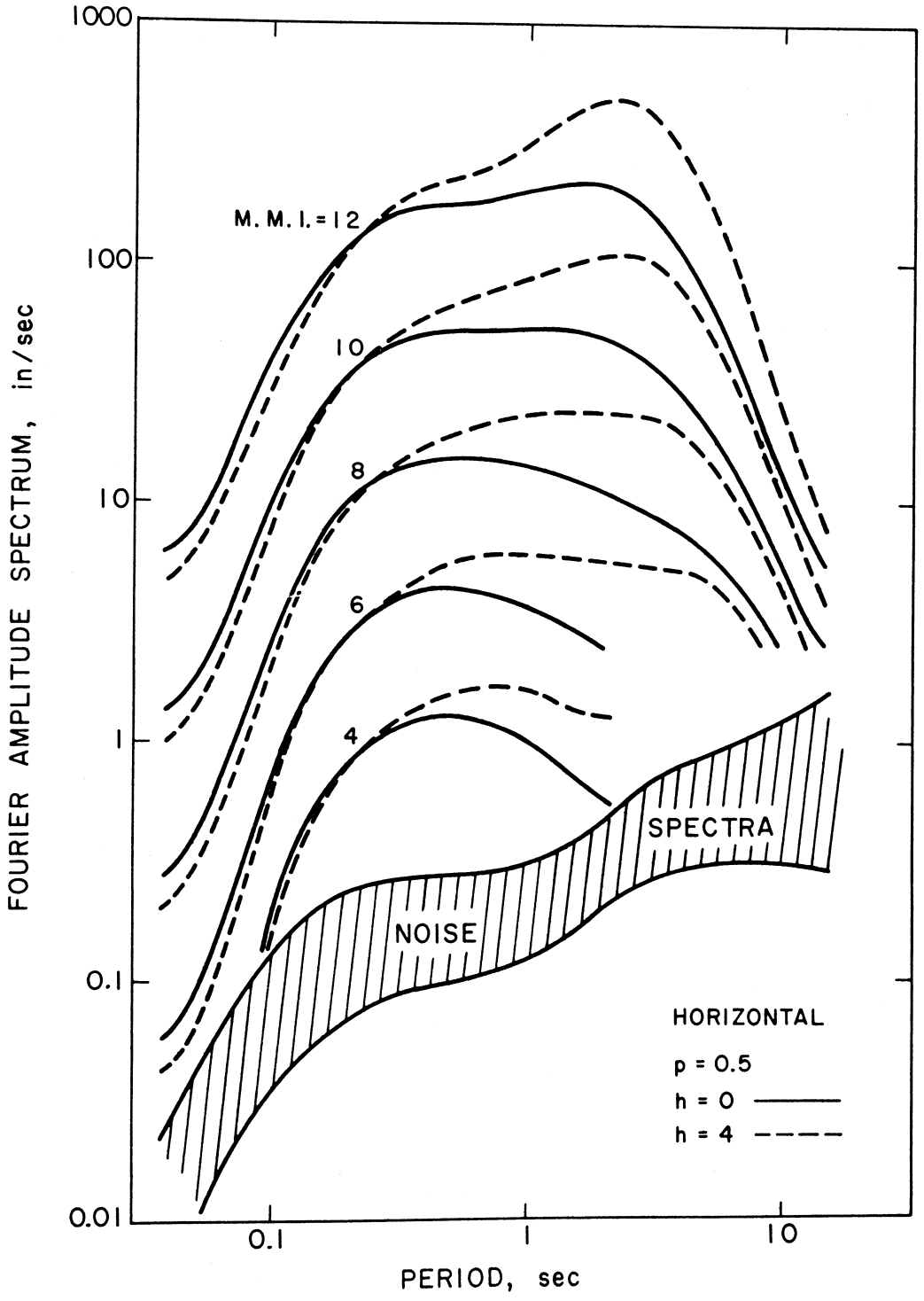

Figure 3.3.3. Average (p = 0.5) Fourier amplitude spectra versus period and for MMI levels IV, VI, VIII, X and XII. h is depth of sediments in km.

in the acceleration data that are based on manual digitization of records between 1933 and 1971.

Strong-motion data are now available at 200 points/sec or a Nyquist frequency of 100 Hz. Advances in the technology of designing strong-motion instruments may eventually lead to increasing the useable frequency from 25 Hz presently to as high at 50 Hz. Thus we need a differentiating formula that is accurate up to that range of frequency, or more generally, that has a transfer function that is accurate up to the variable cutoff frequency and decreases to zero beyond the cutoff frequency.

3.4 Design Criteria for a Differentiation Formula

Based on the previous discussions, we need a differentiation formula that is accurate for data of frequencies up to the variable cutoff frequency, ω_L, discussed in Chapter II.

Let $\lambda = \omega_L/\omega_N$ be the ratio of the cutoff frequency to that of the Nyquist frequency, with $0 < \lambda < 1$. We propose the following criterion for the design of the differentiation filter:

(1) that the filter has the following input-output relationship:

$$\dot{x}[n] = \sum_{-K}^{K} c[k]x[n-k] = \sum_{1}^{K} c[-k](x[n+k]-x[n-k]) \qquad (3.4.1)$$

where $K = K(\lambda)$ is the order of the filter, $c[k] = c[k,\lambda]$, k from -K to K, will be the coefficients of the filter, all of which will depend on λ. The coefficients chosen will be asymmetric, or

$$c[0] = 0, \quad \text{and} \quad c[-k] = -c[k], \qquad (3.4.2)$$

Such a K-th order central difference type formula will give a transfer function that is purely imaginary:

$$H(\omega) = 2i \sum_{1}^{K} c[-k] \sin(k\omega) \qquad (3.4.3)$$

as in the case of the ideal differentiator. (3.4.3) guarantees that there will be no phase distortion from the filter.

(2) that the coefficients c[k] be chosen so that the transfer functions vary smoothly and are close to that of the ideal differentiator in the passband, $0 \leq \omega \leq \omega_L$. No ripples should be present in the transfer function amplitudes in the passband, (section 2.8). The ratio of the normalized filter magnitude, $|H(\omega)/\omega|$, should approach unity tangentially at zero frequency. This will ensure that the error magnitude (3.3.2) in the passband will vary smoothly from zero at zero frequency to an allowable limit at the cutoff frequency. A suitable criteria for this limit may be stated as follows:

(3) that the normalized error magnitude of the differentiator, within the passband, $\varepsilon(\omega)$, satisfies; say

$$|\varepsilon(\omega)| \leq 10^{-3} \qquad 0 \leq \omega \leq \omega_L \qquad (3.4.3)$$

where from (3.3.2)

$$\varepsilon(\omega) = \left| \frac{H(\omega)}{i\omega} - 1. \right|$$

Based on the design criteria set above, we decided to design a class of differentiation filters that are monotone over the frequency band.

Let $H_L(\omega)$ be the smooth nonrecursive lowpass filter given in section 2.9. It has the form

$$H_L(\omega) = b[0] + \sum_{1}^{K} b[k] \cos k\,\omega \simeq \begin{cases} 1 & 0 < \omega < \omega_L \\ 0 & \omega > \omega_L \end{cases} \qquad (3.4.4)$$

Consider the function

$$H_1(\omega) = \sum_{1}^{K} c[k] \cos k\,\omega \qquad (3.4.5)$$

whose coefficients c[k] are defined by

$$c[0] = 0 \qquad c[k] = b[k]/(1 - b[0]) \ , \qquad (3.4.6)$$

so that the function $H_1(\omega)$ again approximates the ideal lowpass filter, with the only difference that it does not have a constant term, c[0]. Consider the differentiator filter, $H_D(\omega)$, given by

$$H_D(\omega) = \sum_{1}^{N} -i\,\frac{c[k]}{k} \sin k \qquad (3.4.7)$$

This is obtained by integrating the "modified" smooth lowpass filter (3.4.5) term by term and multiplying by i. This is a differentiation filter because the integral of the ideal lowpass filter w.r.t. ω

(ideal)

$$H_L(\omega) = \begin{cases} 1 & 0 < \omega < \omega_L \\ 0 & \omega > \omega_L \end{cases} \qquad (3.4.8)$$

is the ideal differentiating filter:

(ideal)

$$H_D(\omega) = \begin{cases} i\omega & 0 < \omega < \omega_L \\ 0 & \omega > \omega_L \end{cases} \qquad (3.4.9)$$

after multiplication by i.

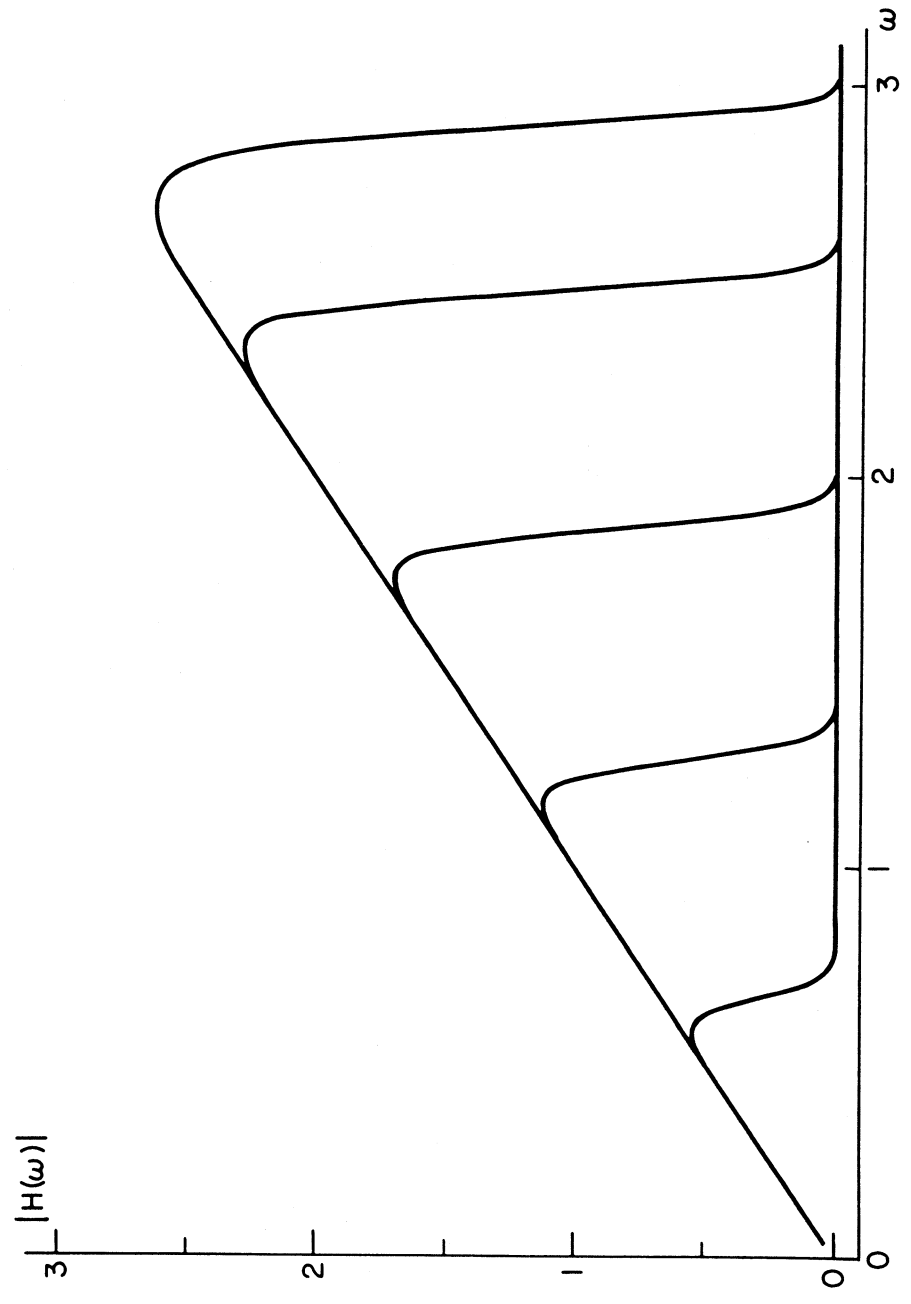

Figure 3.4.1. Differentiation filter amplitudes versus frequency (equation 3.4.7).

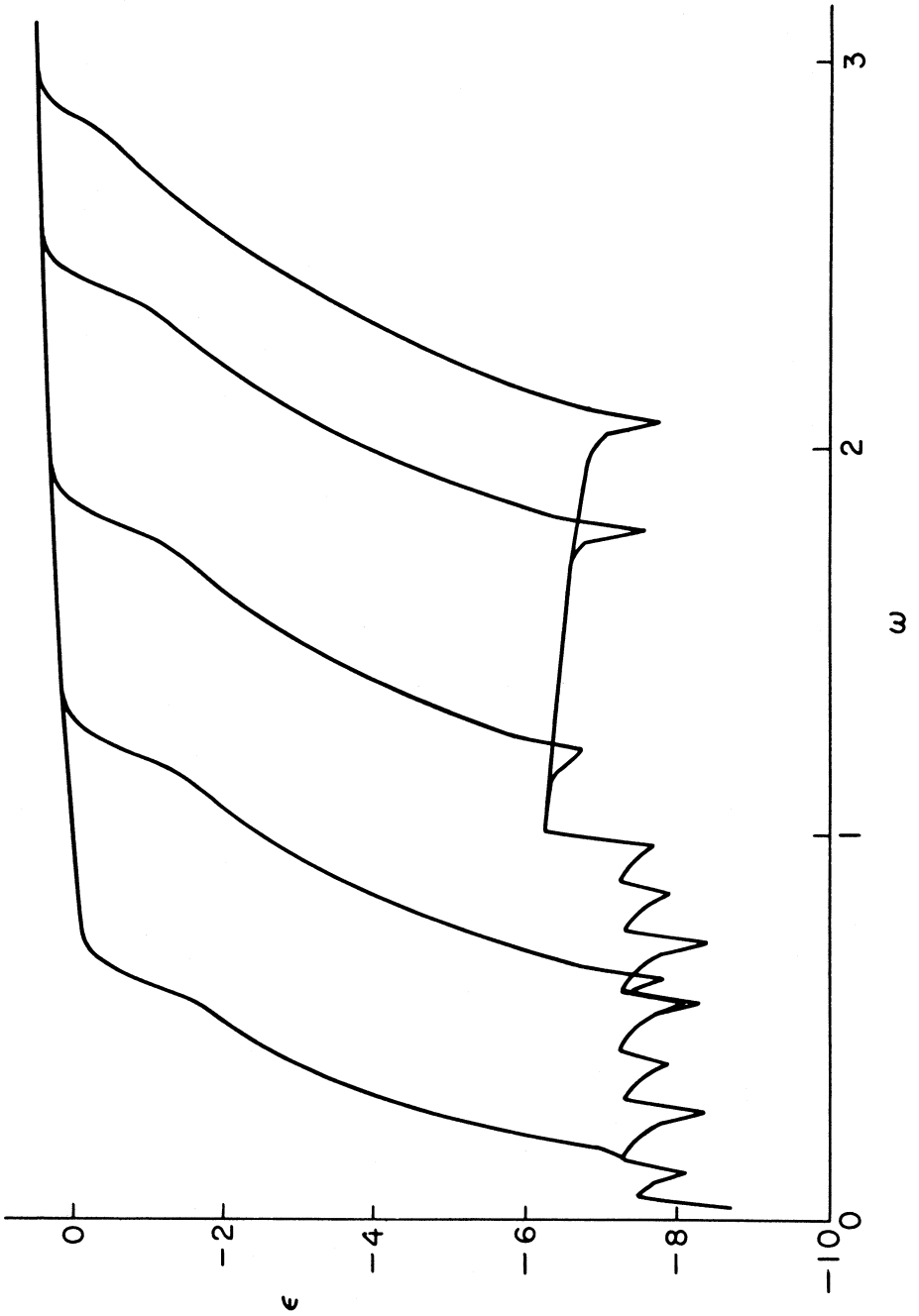

Figure 3.4.2. Normalized error magnitudes for differentiation filters in Figure 3.4.1.

The resulting differentiation filter (3.4.7) is a smooth filter since it is derived from the smooth lowpass filter given in Section 2.9. Figure 3.4.1 shows a plot of the amplitudes versus frequencies for the function at various cutoff frequencies along the frequency band. Each of the functions approximates the ideal differentiator with slope 1 in its passband and then slopes linearly to 0 from the cutoff frequency to the Nyquist frequency. After concantenation with their corresponding smooth lowpass filter, the amplitudes in the plot slope almost vertically to zero in the stop band. The normalized error magnitudes of the functions are given in Fig. 3.4.2. The functions used are well within the design criteria specified above.

CHAPTER IV

BASELINE CORRECTION AND NOISE-FREE CUTOFF PERIOD FOR ACCELERATION, VELOCITY AND DISPLACEMENT

4.1 Introduction

Accelerograms lowpass filtered and corrected for instrument response are next baseline corrected by highpass filtering. For all records, an initial cutoff frequency of 0.07 Hz for the filter is first used. This corresponds to a cutoff period of approximately 14 sec., a sufficiently long period to cover a wide enough band of information for most strong-motion accelerograms (Trifunac et al. 1973). The final cutoff period or frequency band for each accelerogram will be determined separately from the signal-to-noise ratio of each component (Trifunac and Lee, 1979), to be discussed in the second half of this chapter.

Prior to the introduction of the Automatic Record Digitization System (ARDS) (Trifunac and Lee, 1979), with data available only from hand digitization, the accelerogram data after instrument correction were then available at 50 points/sec, equally spaced at 0.02 seconds apart. The routine computer data processing then consists of the procedure for baseline correction (Trifunac, 1970) as follows:

(1) Prior to filtering the instrument corrected data, a straight zero acceleration baseline is least squared fitted to the data to eliminate possible distortions caused by placing the photographic enlargement of the film negatives onto the digitization table.

(2) The data are next lowpass filtered by an equally weighted running mean filter with a window width of 0.04 sec (f = 2.5 Hz).

(3) The lowpass filtered data are decimated and only every tenth point is kept. The decimated data are then at 0.2 sec apart, or at 5 points/sec with a Nyquist frequency of 2.5 Hz. All long period components of periods over 10 sec. are essentially undisturbed.

(4) The decimated data are then used as input to a lowpass Ormsby filter with cutoff frequency of 0.07 Hz. The resulting lowpass filtered data now represent the zero baseline data.

(5) The zero baseline data are interpolated to the original time spacing of 50 points/sec. Straight line interpolation is used.

(6) The baseline corrected data are obtained by subtracting the zero baseline data from the original data.

For data now available at 200 points/sec, or a Nyquist frequency of 100 Hz at this stage, a highpass cutoff frequency in the vicinity of .1 Hz will thus correspond to a ratio of 1 in 1000, or a very small fraction of the whole frequency band of the data. This is thus the problem of narrow band filtering or narrow band rejection. The baseline correction procedure will be reexamined in the next section.

4.2 Narrow Band Filtering

The implementation of a norrow-band filter used to be one of the most difficult problems in digital filtering. This is because such narrow band filters inherently have sharp transitions in their frequency response, thus requiring sophisticated high-order designs to meet the desired frequency response specifications. Those filters usually require lengthy computation in their realizations. Rabiner and Crochiere (1975) showed that efficient implementation of narrow-band filtering by a digital filter can be realized using a sampling

rate reduction (decimation) followed by a sampling rate increase (interpolation). Such decimation and interpolation processes can be efficiently implemented using finite impulse response (FIR) digital filters.

Furthermore, the proposed new procedure has been shown to have the following properties:

(1) The computation (in terms of multiplications per sample) needed to implement the filter is greatly reduced from that required for a standard direct form implementation for an equivalent finite impulse response (FIR) digital filter.

(2) The computation is comparable to that required for optimum (elliptic) infinite impulse response (IIR) filters in a cascade realization.

(3) The phase response can be set to be linear or even zero.

(4) The roundoff noise generated in computing the output can be significantly less than that of a standard direct form FIR implementation.

(5) The coefficient sensitivity problems can be less severe than those for standard direct form FIR implementations.

4.3 Multi-Stage Decimation and Interpolation

For data sampled at 100 to 200 points/sec, a multi-stage (2 or 3) decimation-interpolation for narrow-band FIR filtering has been found to be efficient (Crochiere and Rabiner, 1975). The general procedure for N such stages is as follows:

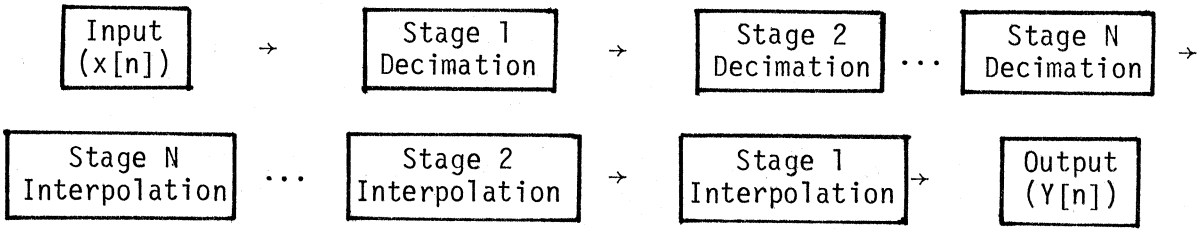

Fig. 4.3.1

At the i-th stage of decimation, let the input signal have a sampling interval of T[i] sec., and the output decimated signal have a sampling rate of T[i+1] = MT[i] sec. The input signal is first lowpass filtered giving the signal w[n]. This is done to avoid aliasing at the larger sampling interval MT[i]. The sampling rate reduction is then achieved by forming a new sequence (y[n]) by extracting every Mth sample of w[n]. A block diagram of this stage is given in Fig. 4.3.2:

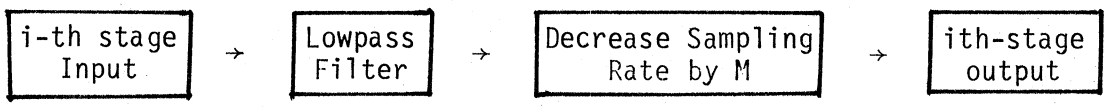

Fig. 4.3.2

The process of interpolating the input signal at the i-th stage of interpolation is similar, as shown in Fig. 4.3.3, where the sampling rate is increased by an integer ratio L, or equivalently, the sampling interval reduced by a factor 1/L, so that T[i+1] = T[i]/L. This is done by first inserting (L-1) zero-valued samples between each sample of y[n]. This will create a signal w[n] having frequency component periodic with period identical to the original sampling period.

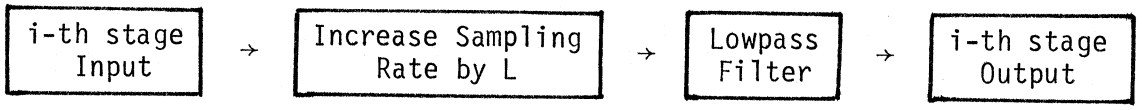

Fig. 4.3.3

The next step is to eliminate these periodic components and retain only the passband frequencies by an appropriate lowpass interpolation filter. The implementation of such filter will be discussed in more detail in the next section. The resulting output signal is then the desired interpolated signal with sampling rate T[i+1] = T[i]/L.

Note that the implementation of such interpolators and decimators involves the use of digital filters in which the input and output sampling rates are different. One of the important considerations in the implementation of such sampling rate changing systems is the choice of the appropriate type of lowpass filters (Rabiner and Good, 1975). For this type of system, a significant savings in computation can be obtained by using a FIR non-recursive filter in a direct form implementation. Such saving in computation is due to the observation that for FIR decimators only one out of each M output samples needs to be calculated, while for FIR interpolators, (L-1) out of every L samples of the input are zero-valued, and thus do not affect the computation. These facts cannot be exploited using the corresponding recursive IIR filters.

4.4 The Interpolation Filter

As mentioned in the previous section, the design of interpolation filters involves the use of lowpass digital filters. Such filters can be designed in a variety of ways, as described in Chapter II, for example, using window designs, equiripple designs, smooth designs, etc. The FIR nonrecursive interpolation filter turns out to be the most

efficient, as described in the previous section. The filter used here is one designed by Oetken et al (1975). It is one in which the mean square criterion is used.

The computer program applies to the design of an interpolation filter in which the sampling rate is increased by an integer factor of L. The resulting filter design allows the original input samples to pass through the interpolator unchanged and it interpolates (L - 1) sample values in between each pair of original samples in such a way that the mean square error between these samples and their ideal values is minimized. The ideal values are the theoretical values predicted by the sampling theorem. The input signal is assumed to be bandlimited, which is always the case for the lowpassed equally spaced accelerogram data.

The original input sample (x[n]) given at the original sampling rate is first converted to one of the new sampling rates (w[n]) as follows:

$$w[n] = \begin{cases} x[n], & n = kL \\ 0, & \text{otherwise} \end{cases} \tag{4.4.1}$$

w[n] is obtained from x[n] by inserting (L - 1) zeros between adjacent samples of the input sample data. Assuming the degree of the filter to be 2LN, the output of the filter y[n], will be

$$y[n] = \sum_j h[j]w[n-j] \tag{4.4.2}$$

where h[j] is the impulse response of the filter. Since w[n] = 0 for $n \neq kL$ according to (4.4.1), for n = kL,

$$y[kL] = \sum_j h[jL]x[(k-j)L] \tag{4.4.3}$$

and for $n = kL + i$, with $i = 1,2,3,\ldots,L - 1$,

$$y[kL+i] = \sum_j h[jL+i]x[(k-j)L] \qquad (4.4.4)$$

which means that for $n = kL$, $y[n]$ will be calculated using only $2N + 1$ samples of $x[n]$ and $h[n]$ and if $n \neq kL$, only $2N$ samples of both sequences will be used.

Examples of the use of the filter to input samples of sine functions at various sampling rates are shown in Fig. 4.4.1, where the original sample points are represented by "0" and the output data are plotted as solid lines. Note that the characteristics of the interpolation filter enable the interpolated data to fill in missing peaks predicted by the sampling theorem that are not present in the original sample.

4.5 The Determination of Cutoff Frequency Band

Having determined and established the use of proper decimation and interpolation filters for baseline correction, we turn to the problem of the determination of the "right" or appropriate cutoff frequency band. As mentioned at the beginning of the chapter, when the routine data processing scheme was first developed, all digitized data were bandpass filtered in the frequency band from 0.07 Hz to 25 Hz (Trifunac, 1971) so that the digitization and processing noise outside the frequency band can be eliminated. The choice of 0.07 Hz and 25 Hz was then based on a detailed study of digitization error characteristics of the digitization system available at the time (Trifunac et al, 1973). These limits then and now do not necessarily apply to records digitized elsewhere with different digitization equipment and processing machines. It is also the case that accelerograms with smaller amplitudes may have a more

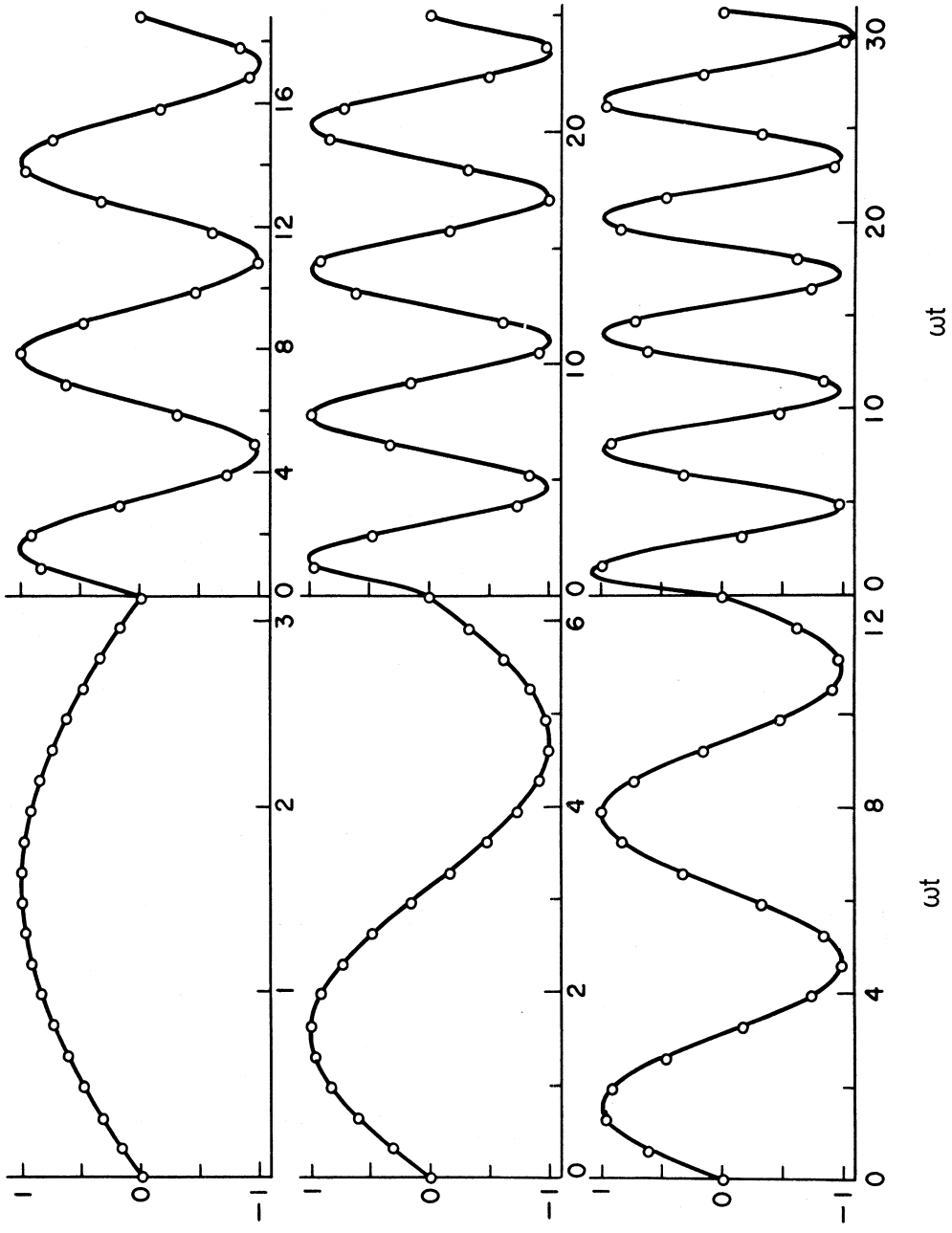

Figure 4.4.1. Interpolation filter (solid lines) and original sample points (small circles).

restricted frequency band within which the signal-to-noise ratio is greater than one.

In the early stage of routine processing, it becomes clear that the optimum bandpass frequency would have to vary from one record to another if one were to eliminate all significant noise from the digitized data. With routine processing of all data in the band 0.07 Hz to 25 Hz, it was known that many records with small amplitudes recorded during small to intermediate earthquakes and at intermediate to large distances will still have a considerable content of digitization and processing noise, especially for periods larger than 1 to 2 seconds. Trifunac (1977) presented an analysis of the first 186 ground motion records, in which he established the frequency bands beyond which the data may be affected by digitization and processing noise.

4.6 An Estimate of Digitization and Processing Noise

Trifunac (1977) presented a method for estimating the digitization and processing noise of a system from which the Response and Fourier amplitude spectra of noise can be calculated. The noise levels for both the manual digitization system and the automatic digitization system (ARDS) have been both analyzed. For the case of the manual system, a thin straight line was digitized separately by several operators. For the automatic system, several SMA-1 accelerograms were used to record straight lines on film and the fixed mirror traces were then digitized as "zero" acceleration records. The resulting digitized traces in both cases were processed as the raw data to obtain the Volume II corrected data at a cutoff frequency band of 0.07 Hz to 25 Hz. The corrected noise data were then used to calculate the Volume III spectral noise data.

Fig. 4.6.1 shows the average and average-plus-one standard deviation of the Fourier (FS) spectral amplitudes for noise records with digitized lengths ranging from 15, 30, 60 to 90 secs. for the automatic digitization system (ARDS). The Fourier Spectrum amplitudes of average digitization noise range from less than 0.01 in/sec. at period, T = 0.04 sec. to almost 5 in/sec. for periods in the range T = 10 to 14 sec. (Fig. 4.6.1). Spectral amplitudes corresponding to average-plus-one standard deviation are almost two times larger.

The above analyses are also carried out for PSV, or pseudo-relative velocity spectra, in the same way as they are for Fourier spectra. Fig. 4.6.2 shows the average and average-plus-one standard deviation of the PSV spectral amplitudes for the same set of noise records calculated at zero damping. These show the same characteristics as the Fourier noise spectra.

The properties of PSV spectra can now be utilized to estimate the noise level of a given component of acceleration. The amplitudes of PSV spectra can be shown to approach the high- and low- frequency asymptotes whose amplitudes are determined by and would correspond to respectively the absolute maximum peak acceleration and maximum peak displacement. When the Fourier spectrum of strong motion is limited to a narrow frequency band, the PSV spectral amplitudes outside this band will tend smoothly towards the asymptotes. In many cases, especially in the long period band, careful inspection of the overall Fourier and Response Spectral shapes and their comparisons with the corresponding amplitudes and trends of noise spectra will help to identify the region where the spectra are dominated by noise.

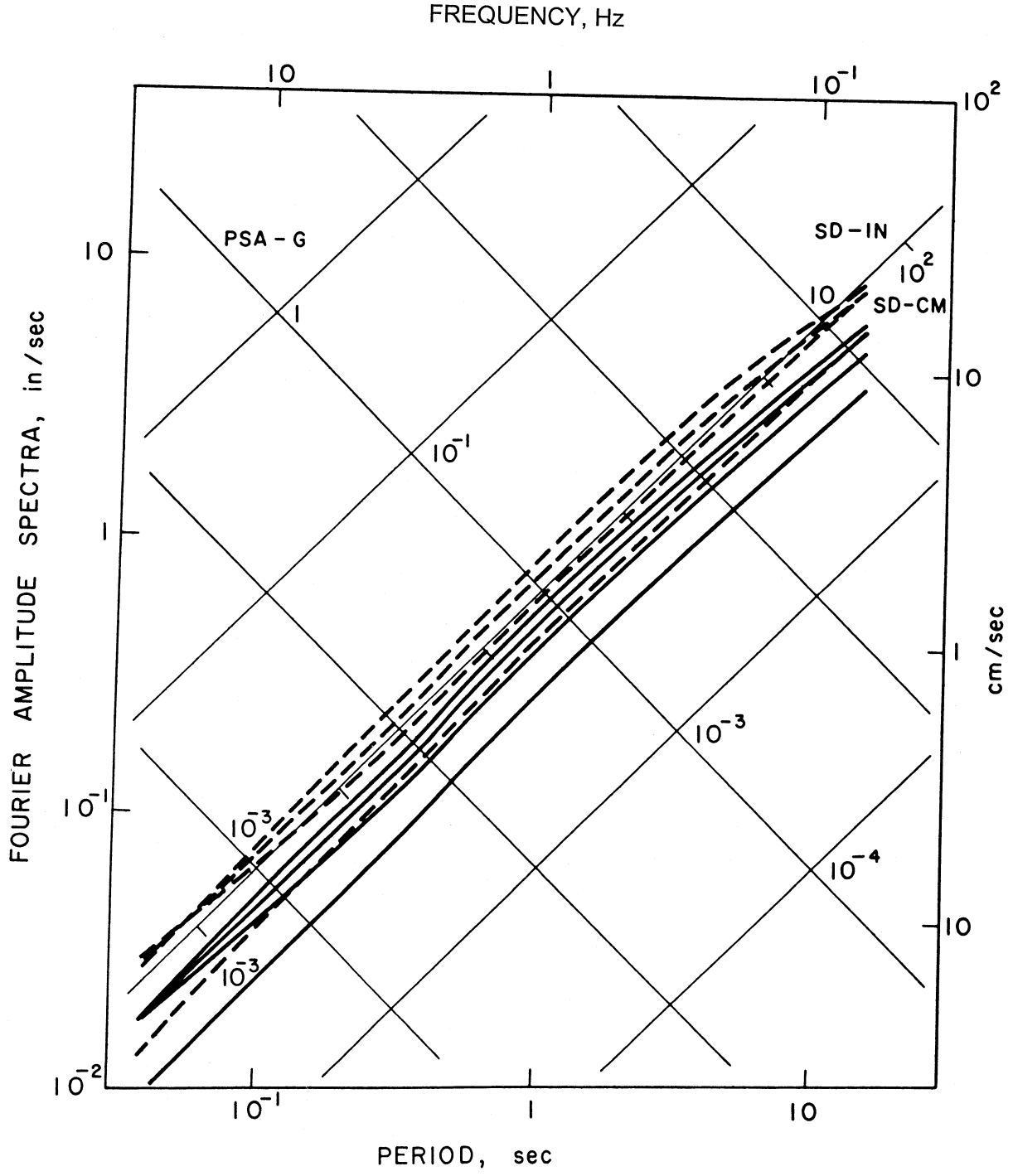

Figure 4.6.1. Average (solid lines) and average plus one standard deviation (dashed lines) Fourier amplitudes of digitization noise for records with duration of 15, 30, 60 and 90 seconds.

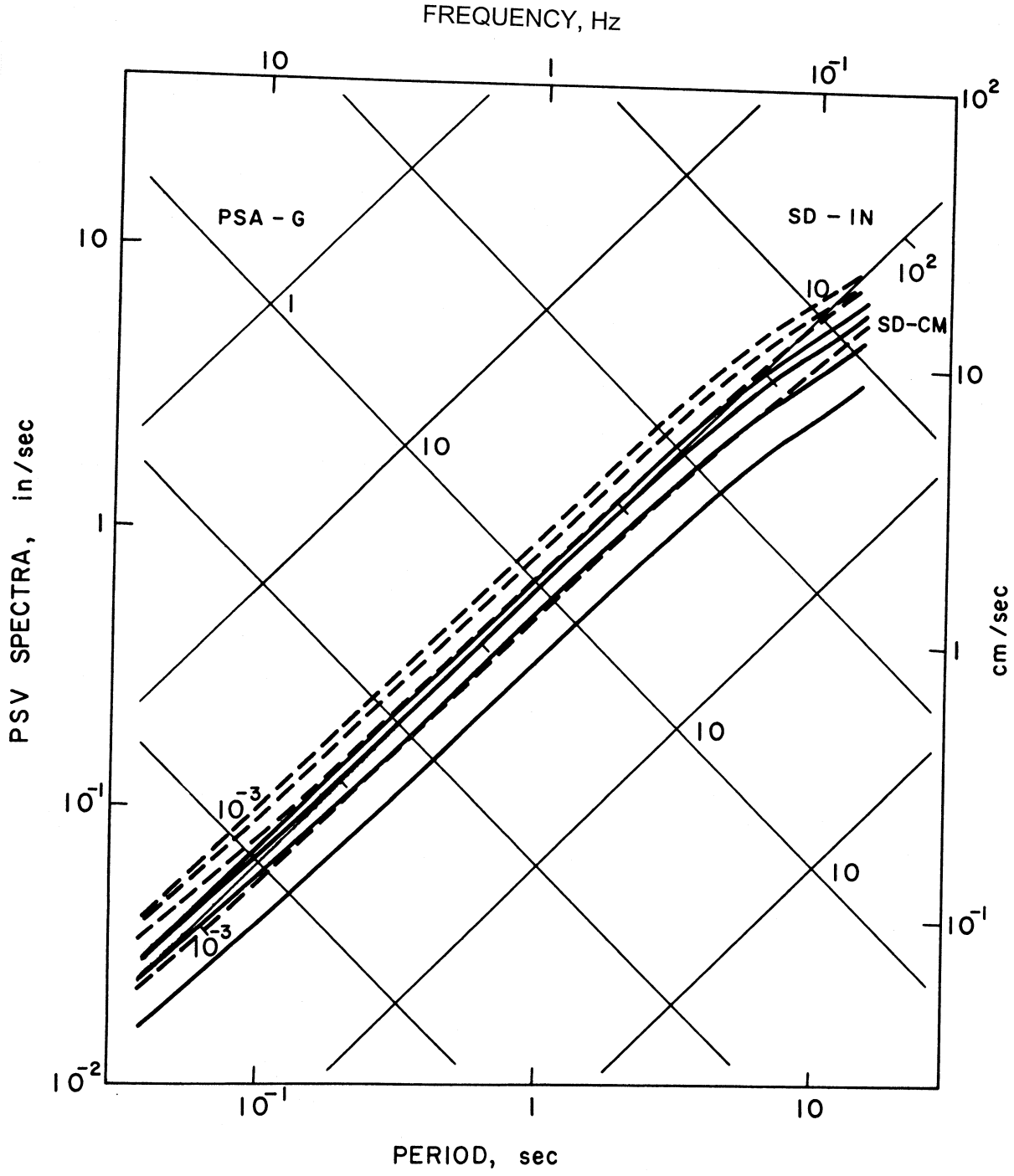

Figure 4.6.2. Average (solid lines) and average plus one standard deviation (dashed lines) PSV amplitudes of digitization noise for records with duration of 15, 30, 60 and 90 seconds.

Since the exact form of Fourier spectra of digitization and processing noise for each individual recording is usually not available, it is not possible to subtract the noise spectra from the processed spectra to obtain the spectra of recorded accelerations only. However, it is usually possible to identify a rather well defined range of periods, which separates those periods T with a large signal-to-noise ratio from those which have a much lower signal-to-noise ratio.

Trifunac and Lee (1978) considered a batch of 186 records which correspond to uniformly processes earthquake ground accelerations in the Western United States of America for the period from 1933 to 1971. These were refiltered with bandpass frequencies predetermined by visual inspection to maximize the signal-to-noise ratio within the band. Of the 186 records or 558 components considered, 69% were originally processed with standard 15 sec. (0.07 Hz) cutoff and the remaining 31% with the 8 sec. (.125 Hz) cutoff. As a result of the above procedure, as much as 50% of the records routinely filtered at 15 sec. were refiltered with a shorter long period cutoff ranging from 1 to 15 sec. Similarly, about 12% of the records routinely filtered at 8 sec. were refiltered with cutoff periods ranging from 1 to 8 sec.

It is also found in many cases, that the signal-to-noise ratio at the high frequency (short period) end also becomes small for many accelerograms which were recorded during small earthquakes and/or at greater epicentral distances.

4.7 A Computer Subroutine for the Determination of the Noise-Free Band

It might appear difficult at present, as it was in the late 60's and early 70's to select an optimum long period cutoff for standard routine data processing scheme. No such one cutoff period for all

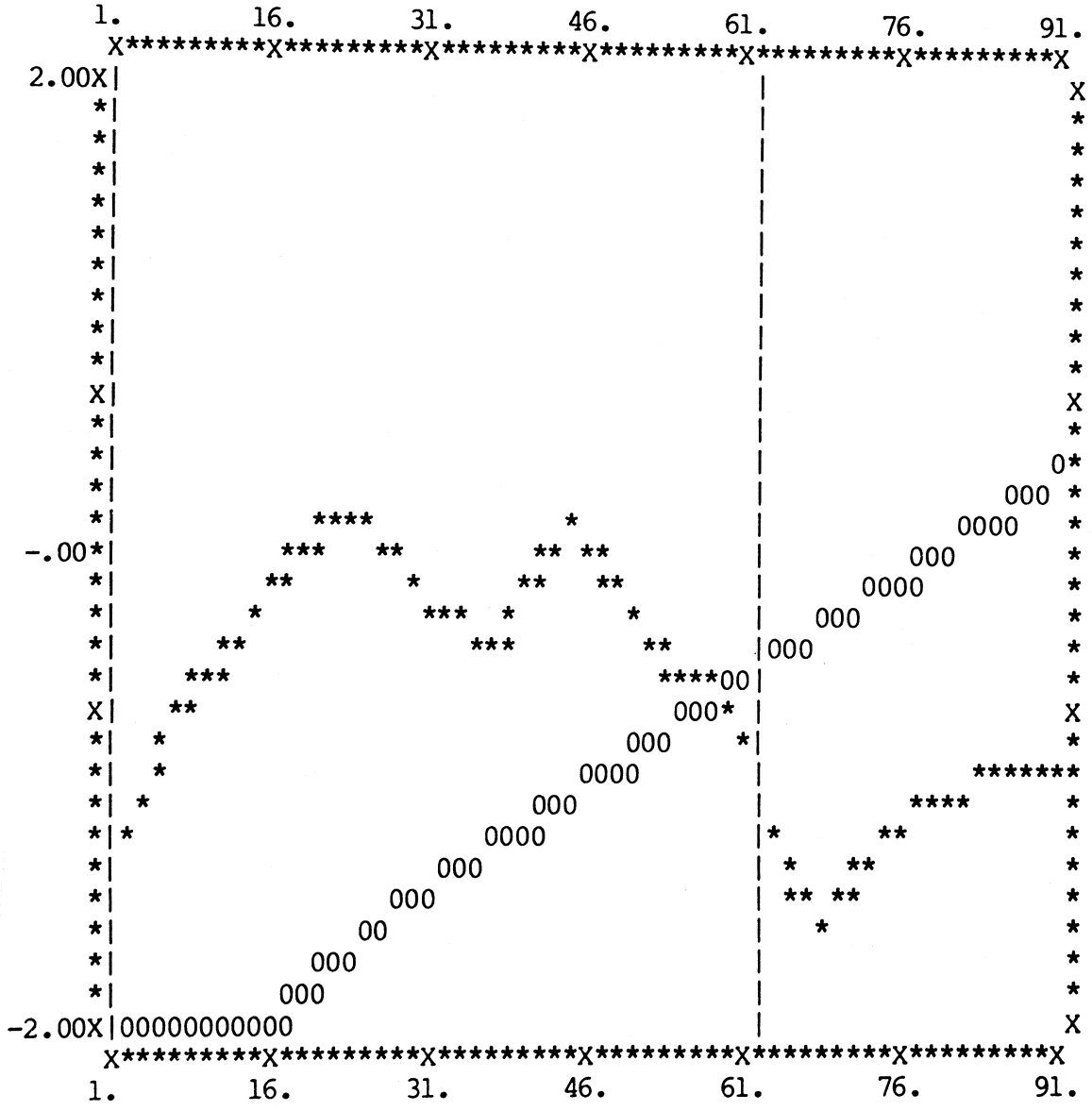

Figure 4.7.1. Selection of long period cutoff for chosen signal to noise ratio equal to one.

records can be selected to satisfy the requirements of all future analyses which will or need to use the corrected strong-motion accelerograms. It becomes clear, however, that in the routine data processing scheme, a step has to be included to have a computer subroutine determine automatically the frequency band that is as free from noise as possible, and a subsequent step to refilter the data at this new cutoff frequency band. The resulting strong-motion acceleration data from routine processing will now have a variable cutoff frequency band that normally depends on the amplitudes of the strong-motion, which in turn depends on the magnitudes of the earthquake, the local geology and epicenteral distance of the site from the source.

Fig. 4.7.1 shows an example of the current computer output at the step where the Fourier amplitudes of the input acceleration are calculated and compared with that of the digitization noise of the same length. A simple line-printer plot shows the automatic determination of the cutoff frequency band by the computer subroutine which in this case is shorter than the usual 15 sec. cutoff period.

4.8 Computation of Velocity and Displacement

With the digital acceleration data bandpass filtered and instrument corrected, integration is the next step of data processing to complete the calculation of the velocity and displacement curves. The calculation of the velocity and displacement data from an accelerogram is not a trivial matter (Hudson, 1970). Early in the 1960's a number of studies of the best way of carrying out the integrations have been made (Hudson, 1963; Berg, 1963; Brady, 1966; Amin and Ang, 1966; Schiff and Bogdanoff, 1967). In the 1970's most methods employ digital computations and

certain correction techniques for long period errors resulting from integration (Trifunac and Lee, 1973).

Hudson (1970) listed several important reasons for the computation of velocity and displacement data with resonable accuracy. Edwards and Northwood (1959) and Neumann (1958) showed that for blast loading the single best descriptive number related to structural damage is the maximum ground velocity. Neumann (1959) also showed that the maximum ground velocity can be correlated approximately with the Modified Mercalli Intensity Scale, a scale commonly used to give a round measure of the damage associated with strong earthquakes. In a similar fashion, the ground displacement data also has practical application because of the direct relationship between ground displacements and the strain to which large structures such as dams and underground pipelines might be subjected.

4.9 Digital Integration

The data processing program developed originally for the manually digitized data (Trifunac and Lee, 1973) used the trapezoidal rule of integration,

$$y[n+1] = y[n]+.5T(x[n]+x[n+1]) \qquad (4.9.1)$$

with (x[n]) representing the input and (y[n]) the output digital data, T is the equally spaced sampling time of the sequence in seconds. Since y occurs on both sides of this equation, this is a recursive filter.

Again, as in the case of differentiation formulae (Section 3.1), with data originally interpolated to 100 points/sec., the trapezoidal rule is good for data up to frequencies of about 15 Hz. We again examine the numerical integration formulae in the frequency domain, which

then becomes the problem of designing a filter to estimate the integral of digital data. The integration filter is to be designed as a linear time-invariant system, where the complex exponential functions, $\exp(i\omega t)$, are again eigenfunctions (Section 3.2). The equation for the integral

$$\int \exp(i\omega t)dt = \frac{1}{i\omega} \exp(i\omega t) \ , \tag{4.9.2}$$

gives the transfer function of the integration filter as (for T=1)

$$H(\omega) = \frac{1}{i\omega} \tag{4.9.3}$$

for $-\pi \leq \omega \leq \pi$. The ideal integrator with curoff frequency, ω_c, has a transfer function similarly given by

$$H_I(\omega) = \begin{cases} \frac{1}{i\omega} & |\omega| < \omega_c \\ 0 & \omega_c < |\omega| < \pi \end{cases} \tag{4.9.4}$$

Note from equations (4.9.3) and (4.9.4) that the phase of the integration filter is $-\pi/2$. The filter corresponding to the trapezoidal rule (4.9.1), by assuming the input $x(t)$ as $e^{i\omega t}$ and the corresponding output $y(t)$ as $H(\omega)e^{i\omega t}$, has a transfer function

$$H(\omega) = \frac{1}{2} \frac{(e^{i\omega}+1)}{(e^{i\omega}-1)}$$

or

$$= \frac{\cos \frac{\omega}{2}}{2i \sin \frac{\omega}{2}} \ , \tag{4.9.5}$$

which approaches $\frac{1}{i\omega}$ as $\omega \to 0$, but gradually decreases to zero as $\omega \to \pi$, the Nyquist frequency. This means that, like most common integration

formulae, the frequency response function of the integrator will not differ significantly from the ideal response at frequencies much less than the Nyquist frequency. If the input to an integrator is band limited to frequencies less than the Nyquist frequency, theory shows that it should be able to integrate the function exactly. Exact integration will, however, require the entire input time history. Integration formulae with a finite number of filter weights should therefore be designed to have a frequency response within the passband frequency as close to the ideal one as possible.

Sunder (1980) proposed the use of an integration formula (Schussler-Iber) of the form:

$$y[n+1] = y[n] + (\frac{T}{3}) \sum_{k=0}^{7} b[k]x[n+1-k], \qquad (4.9.6)$$

with $b[k] = b[7-k]$. The phase of the corresponding filter, however, is not $-\pi/2$, unlike the case of the ideal integrator. Hence the use of the filter will produce a phase distorted output, which is objectionable for data processing in earthquake engineering.

4.10 Designing a Digital Integrator

To choose an appropriate integration formula, let $y(t)$ be the integral of a function $x(t)$:

$$y(t) = \int_{o}^{t} x(u)du \qquad (4.10.1)$$

where $x(t) = 0$ for $t < 0$ and $t \geq NT$. The function $x(t)$ is sampled at equally spaced interval of T sec., $\{x[n]\}$, with $x[n] = x(nT)$, $n=0,1,2,...$ Integrating the function in steps of T seconds, we can write

$$y[n+1] = y[n] + \int_{nT}^{(n+1)T} x(t)dt \qquad (4.10.2)$$

The portion of the function $x(t)$ for $nT \leq t \leq (n+1)T$ can be reconstructed, say, from the sequence $\{x[n+k]\}$, for k from $-K+1$ to $+K$, using some form of reconstruction formula,

$$x(t) = \sum_{k=-K+1}^{K} x[n+k]h(t-(n-k)T), \qquad (4.10.3)$$

where $h(t)$ is the inpulse response of the reconstruction filter. Note that when $K=\infty$, the Whittaker reconstruction filter will be one such filter.

Substituting (4.10.3) into (4.10.2) gives

$$y[n+1] = y[n] + \sum_{k=-K+1}^{K} b[k]x[n+k] , \qquad (4.10.4)$$

where

$$b[k] = \int_{0}^{T} h(t+kT)dt \qquad (4.10.5)$$

To ensure that the corresponding filter has a phase shift of $-\pi/2$, we need

$$b[k] = b[-k+1] \qquad (4.10.6)$$

$k=1$ to K, so that

$$y[n+1] = y[n] + \sum_{k=1}^{K} b[k](x[n+k] + x[n-k+1]) \qquad (4.10.7)$$

Choosing $x(t)$ as $e^{i\omega t}$ and $y(t)$ and $H(\omega)e^{i\omega t}$, the transfer function of the filter is given by

$$H(\omega) = \frac{\sum_{k=1}^{K} b[k](e^{ik\omega} + e^{-i(k-1)\omega})}{e^{i\omega}-1}$$

$$= \sum_{k=1}^{K} \frac{b[k]\cos(k-\frac{1}{2})\omega}{i \sin\frac{\omega}{2}} \qquad (4.10.8)$$

which shows that the filter indeed has the right phase of $-\pi/2$. Note that trapezoidal rule is a special case of this with K=1 and b[1]=.5 (T=1).

As in the case of differentiation, we propose the use of the integration filter that is accurate for data of frequencies up to the predetermined variable cutoff frequency, ω_L. Again, let $\lambda = \omega_L/\omega_N$, the ratio of the cutoff frequency to that of the Nyquist frequency. With $0 < \lambda < 1$. We propose the following criteria for the design of the integration filter:

(1) That the filter be of the form (4.10.4)

$$y[n+1] = y[n] + \sum_{k=-K+1}^{K} b[k]x[n+k]$$

where $K=K(\lambda)$, the order of the filter, $b[k])=b[k,\lambda]$, k=-K+1 to K, the coefficients of the filter, will all depend on λ. The coefficients will satisfy b[k]=b[-k+1], for k=1,2,3,...,K, so that the phase of the filter will be $-\pi/2$, as in the case of the ideal integrator. This will ensure no phase distortion.

(2) That the coefficients $b[k]=b[k,\lambda]$ be chosen so that the resulting filter (4.10.8) will be as close to the ideal one as possible within the passband of the frequency bandwidth.

(3) That the filter be as smooth as possible, the magnitude of the transfer function should be free from ripples in both the pass- and stopband.

(4) That the ratio |design filter/ideal filter| should approach 1 as $\omega \to 0$, so that both have the same tangency at $\omega = 0$.

With appropriate digital integration performed on the acceleration data to get the velocity data, the computed velocity data is next high pass filtered using the same procedure with the same cutoff as in the case of the acceleration data. This is performed to eliminate any long period error resulting from the integration and resulting from the uncertainties involved in estimating the initial velocity of ground motion (Hudson, et al., 1971). The same baseline correction is carried out for the displacement data obtained from integrating the velocity data. Thus, the final step of Volume II data processing is now completed.

CHAPTER V
CONCLUDING NOTES

5.1 Updating Volume III Data Processing

The Volume III data processing consists of calculating the Fourier and Response spectra of single-degree-of-freedom systems for chosen 91 natural periods and 5 dampings from the Volume II corrected accelerogram data. The existing algorithm uses an approach based on the exact analytical solution of the Duhamel integral for successive linear segments of excitation. Such typical Response calculation of a single-degree-of-freedom system uses a recursive algorithm for calculating $\{x[n+1],\dot{x}[n+1]\}$ from $\{x[n];\dot{x}[n]\}$ and the acceleration $\{a[n],a[n+1]\}$. Each time step of the iteration requires 8 multiplications and 6 additions. For a typical acceleration of 60 seconds at 50 points/sec., or 30 seconds at 100 points/sec., or 15 seconds at 200 points/sec., or about 3000 points of data, this would imply that:

Total # of iteration steps = 5 x 91 x 3,000 = 1,365,000,

and for using the existing algorithm, this will mean

Total # of multiplications = 1,365,000 x 8 = 10,920,000

Total # of additions = 1,365,000 x 6 = 8,190,000.

A new algorithm using the digital impulse invariant and step invariant simulation of a continuous system has been derived which requires only 2 multiplications and 3 additions at each step of iteration. This amounts to a 75% saving in multiplication and 50% saving in addition of CPU time. For the same given 3000 points of acceleration, this will mean, using the new algorithm:

Total # of multiplications = 1,365,000 x 2 = 2,730,000

Total # of additions = 1,365,000 x 3 = 4,095,000.

The accuracy of the new algorithm is guaranteed by the sampling theorem in digital signal analysis. For a complete description of this algorithm, the reader is referred to the paper (Lee, 1984): "A New Fast Algorithm for the Calculation of Response of a Single-Degree-of-Freedom System to Arbitrary Load in Time."

5.2 Batch Model Data Processing

Batch mode data processing involves efficient execution of the Volume I, II and III data processing programs with minimal user's iteration and the least possible amount of required input from the user. The existing Volume I processing stage requires the input of earthquake, station and accelerogram information for each component of each record, a step which is often repeated unnesessarily in routine processing of records from the same earthquake or station. It is thus appropriate to set up an information file for earthquake, "EQUAKE.INFO," say, and similarly one for the existing stations, "STATION.INFO," to be used with all the necessary information on files. Processing the Volume I stage will then involve only referring to the appropriate earthquake and system reference numbers each time. This will enable batch mode Volume I processing.

With the use of appropriate filters for lowpass filtering, instrument and baseline correction, the automatic determination of the cutoff frequencies for bandpass filtering and the use of appropriate integration filter, all described in detail in previous sections, the batch mode

Volume II processing is now possible and completed. Currently, the Volume III processing at USC is also available in batch mode. This will thus allow one batch job for successive Volume I, II and III processing. This will provide an efficient prototype for data processing of a large data load.

5.3 Conclusion

The results of this effort, we hope, should be of considerable value for the engineering community. Our aim has been to provide a set of guidelines for different steps in data processing, for the design and efficient use of the necessary filters and an efficient prototype for data processing of a large data load. The possibility of batch mode automatic processing will also allow outside users to access the computer where the programs are to do data processing without any difficulty.

APPENDIX A

THE UPDATED AUTOMATIC ROUTINE DIGITIZATION SYSTEM (ARDS) II

This appendix describes the recent improvements in the automatic digitization programs since the last reported improvements outlined in Appendix A of Lee and Trifunac (1982): EQINFOS (The Strong-Motion Earthquake Data Information System). The Automatic Routine Digitization System (ARDS) was originally developed at U.S.C. (Trifunac and Lee, 1979). Numerous improvements have been implemented and further developed through the actual use of the ARDS in digitization of several recent "difficult" records.

A1 The Program "MAKGAP"

The Imperial Valley, California earthquake of October 15, 1979 was recorded at the Route 8/Meloland overpass by 26 transducers distributed among two central-recording (CR-1) stations. Each of these stations registered 13 acceleration traces. The unit which recorded traces 1 through 13 malfunctioned, and at about every 2 or 3 seconds the uniform film motion with nominal speed of 1 cm/sec. was interrupted. Most of these interruptions each lasted from less than to about 1/4 seconds. Between the interruptions the film motion was fairly uniform and apparently had uniform velocity. Table I gives the estimated durations of these interruptions.

To reconstruct the motions recorded on this film it was necessary to develop a new program (MAKGAP) which was designed to work with other routine programs for automatic digitization (Trifunac and Lee, 1979). The details of this digitization process are outlined in the report

TABLE 1

Time of occurrences, duration and pixel width of interruptions for Rte 8/ Meloland Overpass records, Imperial Valley 15 October 1979.

Interruption No.	Time after triggering (seconds)	Duration of stall (seconds)	Width (No. of pixels)
1	2.65	.13	26
2	5.60	.04	8
3	8.55	.25	51
4	11.15	.05	10
5	14.30	.04	8
6	17.35	.22	44
7	20.05	.19	38

entitled "Automatic Digitization and Processing of Strong Motion Accelerograms" by Trifunac and Lee (1979) and need not be repeated here. For completeness and clarity of this presentation we mention only several key characteristics of this package so that the reader of this appendix can understand the procedures required for processing of records with interruptions.

Digitization of accelerograms is accomplished in three steps. The first step, run by the program called FILM (Trifunac and Lee, 1979) maps the pixels read off the film, with the light transmission intensity greater than a chosen threshold level, onto a disk file. While this is done, the operator, to speed up later operations, supplies the markers which identify the onset and the type of different traces (e.g. time trace, fixed trace, fiducial marks, common edges, etc.) As digitization progresses further the operator also inserts the flags (marked by the left pointing arrows and letter T, to designate the locations where the film motion stopped for a short time interval. The original recording appears as the trace marked ABCD in Figure A1.1, for example. After digitization is completed the program MAKGAP is initiated to insert the desired blank pixel bands along the y-axis and with the width which corresponds to the duration of the stall multiplied by 200. This is because the pixel sizes are 50μ by 50μ square and the film speed of 1 cm/sec. i.e. there are 200 digitized points per second.

The location and the duration of the stalls will be determined by the careful analysis of the half second time trace and the recorded accelerations. Typically there will appear a consistent bulge on all traces at a given X location every time the recording light beams would become stationary in X, during a stall. This is easily seen on the

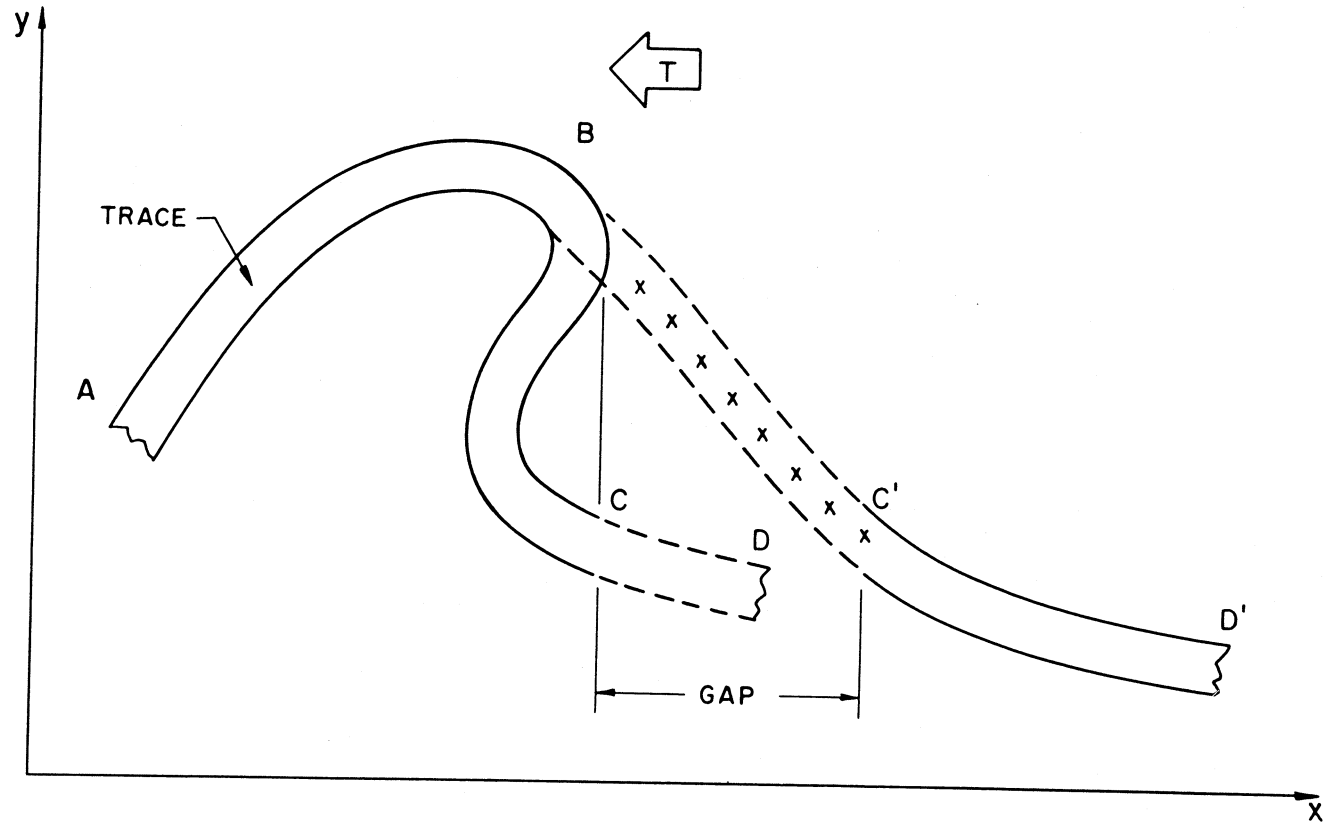

Figure A1.1. Trace appearance at a stall (ABCD). Program MAKGAP inserts desired number of blank pixel bands along y-axis with GAP width corresponding to the duration of stall.

original film. An example of how this stall shows up on a time trace is shown in Figure A1.2.

If the duration of a stall is longer than 1/2 second it is not possible to determine its actual duration since a multiple of 1/2 second could always be added without altering the appearance of the recorded time trace (Figure A1.2).

After the program MAKGAP is executed the data in Figure 2 appears as ABC'D' with a gap n pixels wide. This is repeated at each X where the operator marked a gap by the arrow with "T." For the records described here there were 7 such gaps during the first 22 seconds of strong motion (Table 1).

During the second stage of data processing the digitized data on disk file SCANS is automatically analyzed by the program TRACE and a center of each line is connected by a continuous curve. This process goes on for all X and for all traces of the original film as long as there are no gaps or difficult trace intersections (Trifunac and Lee, 1979). When a gap is encountered, TRACE terminates the line definition on the left wide of a gap, opens new file for a new line which is created on the right side of the gap and the process continues.

During the third part of the digitization process the program TV is used by the operator to fix the difficult places on the film and to correct any errors. Referring to Figure 1 the operator now cuts the trace ABCD at B and deletes section BCD. Then he creates reasonable trace form between B and C' (indicated by + between B and C' in Figure A1.1), connects B with C' and creates a continuous trace ABC'D'. This process is repeated at each of the gap locations for all acceleration traces and for all fixed and other traces present on the film).

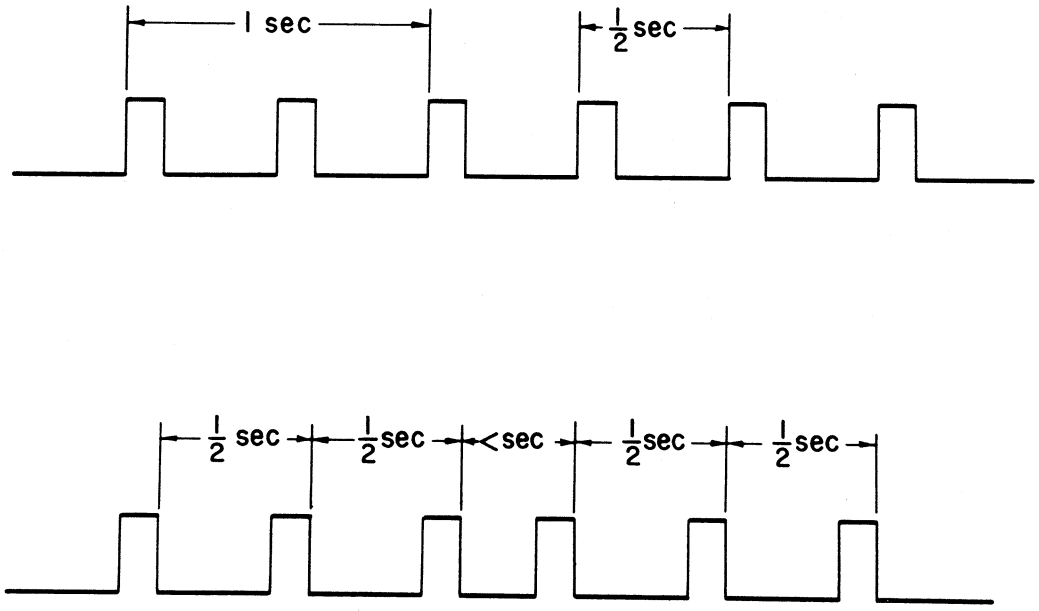

Figure A1.2. Normal, uniform time trace (top). Time trace with stalls will have intervals shorter than 1/2 second (bottom).

When the editing work is completed the data is written onto a disk file format for volume 1 processing by means of program SCRIBE (Trifunac and Lee 1979). Subsequent steps involve the volume 1, 2, and 3 processing, creation of the complete heading data for each trace and copying of all desired files onto a magnetic tape for distribution. The principles of this operation as well as the detailed listings of the programs used for this purpose are contained in the USC report CE 79-15 II by Lee and Trifunac (1979).

The above procedure is not unique and different operators would interpret the acceleration amplitudes within the gaps differently. However, the relatively short duration of most admissible gaps and clearly visible limits of maximum and minimum excursions of recorded acceleration during the gaps will not be difficult to interpret so that the errors in the final digitized data, though certainly present, should be "very small."

A2 The Program "DFILM"

Due to the poor, nonuniform or worn-out quality of some films, which are used to record in analog recording instruments, or because of possible problems that may result during the chemical processing of the film, the developed film may often result in having non-uniform exposure, so that some parts of the record may appear lighter or darker than the other parts.

The first step of digitization, currently executed by the program called FILM (Trifunac and Lee, 1979) allows the user to set the conveniant threshold levels for up to four different sections of the film, ranging from bottom to top. This means that in each section, the same

threshold cutoff level will be used all across the film from left to right ends. When the background optical density of film is not uniform, however, this will create problems. This may result, for example, in having the normal portions of the record well digitized, but areas with lighter background digitized with excessive points from noise or scratches on the film.

A new version of the program, called "DFILM" has now been developed where the program calculates periodically the average threshold level of the section just digitized and updates the threshold cutoff level to a predefined linear function of the average level. "DFILM" can update this threshold cutoff level at up to four different sections of the film from top to bottom. This new program has been tested on film records with non-uniform brightness and has been found to be an efficient way to digitize such records.

REFERENCES

Alford, J. L., G. W. Housner and R. R. Martel (1951). Spectrum Analysis of Strong Motion Earthquakes, EERL, Calif. Inst. of Tech., Pasadena.

Amin, M., and A.H.S. Ang (1966). A Non-Stationary Stochastic Model for Strong-Motion Earthquakes, Structural Research Series No. 306, University of Illinois, Urbana.

Anders, E. B., J. J. Johnson, A. D. Lasaine, P. W. Spikes and J. T. Taylor (1964). Digital Filters, NASA Contr. Rep. CR-136.

Berg, G. V. (1963). A Study of Error in Response Spectrum Analysis, Primeras Jornadas Chilenas de Sismologia & Ingenieria Antisismica, Vol. I., Asociacion Chilena de Sismologia & Ingenieria Antisismica, Santiago.

Biot, M. A. (1941). A Mechanical Analyzer for the Prediction of Earthquake Stresses, Bull. Seism. Soc. Amer., 31, 151-171.

Brady, A. G. (1966). Studies of Response to Earthquake Ground Motion, EERL Calif. Inst. of Tech., Pasadena.

Edwards, A. T. and T. D. Northwood (1959). Experimental Blasting Studies on Structures, Ottawa: Hydro-Electric Power Commission of Ontario and National Research Council.

Gold, B. and C. M. Rader (1975). Digital Processing of Signals, McGraw-Hill, New York.

Hamming, R. W. (1962). Numerical Methods for Scientists and Engineers, McGraw-Hill, New York.

Hamming, R. W. (1977). Digital Filters, Prentice Hall, New Jersey.

Housner, G. W. (1947). Ground Displacement Computed from Strong-Motion Accelerograms, Bull. Seism. Soc. Amer., 37, 299-305.

Hudson, D. E. (1963). The measurement of Ground Motion of Destructive Earthquakes, Bulletin of the Seismological Society of America, Vol. 53, No. 2, February.

Hudson, D. E., N. C. Nigam and M. D. Trifunac (1969). Analysis of Strong Motion Accelerograph Records, Fourth World Conf. on Earthquake Engineering, Santiago, Chile.

Hudson, D. E. (1970). Ground Motion Measurements, Earthquake Engineering, R. L. Wiegel Coordinating Editor, Chapter 6, Prentice-Hall, Inc., Englewood Cliffs, N. J.

Hudson, D. E., M. D. Trifunac, A. G. Brady and A. Vijayaraghavan (1971), Strong Motion Earthquake Accelerograms, II, Corrected Acceleration and Integrated Velocity and Displacement Curves, EERL 71-50, Calif. Inst. of Tech., Pasadena.

Hudson, D. E., M. D. Trifunac and A. G. Brady (1972). Analyses of Strong Motion Earthquake Accelerograms, Response Spectra, Vol. III, Part A, EERL 72-80, Calif. Inst. of Tech., Pasadena.

Hudson, D. E. (1984). Golden Anniversary Workshop on Strong Motion Seismology, March 30-31, 1983, Dept. of Civil Eng., University of Southern California, Los Angeles.

Lee, V. W. and M. D. Trifunac (1982). EQINFOS (The Strong-Motion Earthquake Data Information System), Dept. of Civil Engineering, Report No. CE 82-01, University of Southern California, Los Angeles, California.

Lee, V. W. (1984). A New Fast Algorithm for the Calculation of Response of a Single-Degree-of-Freedom System to Arbitrary Load in Time. Int. J. of Earthquake Engineering and Soil Dynamics.

Neumann, F. (1958). Damaging Earthquake and Blast Vibrations, The Trend in Engineering, Seattle: University of Washington.

Neumann, F. (1959). Seismological Aspects of the Earthquake Engineering Problem, Proceedings of the 3rd Northwest Conference of Structural Engineering, State College of Washington.

Oetken, G., T. W. Parks and H. W. Schuster (1975). New Results in the Design of Digital Interpolators, IEEE Trans. on Acoustics, Speech and Signal Processing, Vol. ASSP-23, No. 3, June.

Oppenheim, A. V. and R. W. Schafer (1975). Digital Signal Processing, Prentice Hall, New Jersey.

Rabiner, L. R. and R. E. Chochiere (1975). A Novel Implementation for Narrow-Band FIR Digital Filters, IEEE Trans. on Acoustics, Speech and Signal Processing, Vol. ASSP-23, No. 5, Oct.

Rabiner, L. R. and B. Gold (1975). Theory and Application of Digital Signal Processing, Prentice Hall, New Jersey.

Schiff, A., and J. L. Bogdanoff (1967). Analysis of Current Methods of Interpreting Strong Motion Accelerograms, Bull. Seism. Soc. Amer., Vol. 57, No. 5.

Sunder, S. S. (1980). On the Standard Processing of Strong-Motion Earthquake Signals, Ph.D. Thesis, Research Report R80-38, School of Engineering, Mass. Inst. of Technology, Cambridge, Mass.

Trifunac, M. D. (1971). Zero Baseline Correction of Strong-Motion Accelerograms, Bull. Seism. Soc. Amer., 61, 1201-1211.

Trifunac, M. D. (1972). A Note on Correction of Strong-Motion Accelerograms for Instrument Response, Bull. Seism. Soc. Amer., 62, 401-409.

Trifunac, M. D. (1973). Analysis of Strong Earthquake Ground Motion for Prediction of Response Spectra, Int. J. of Earthquake Eng. and Struct. Dynamics, Vol. 2, No. 1, 59-69.

Trifunac, M. D. and D. E. Hudson (1970). Laboratory Evaluation and Instrument Corrections of Strong Motion Accelerographs, EERL 70-04, Calif. Inst. of Tech., Pasadena.

Trifunac, M. D., F. E. Udwadia and A. G. Brady (1971). High Frequency Errors and Instrument Corrections of Strong Motion Accelerograms, Earthquake Eng. Res. Lab., EERL 71-05, Calif. Inst. of Tech., Pasadena.

Trifunac, M. D., F. E. Udwadia and A. G. Brady (1973). Analysis of Errors in Digitized Strong Motion Accelerograms, Bull. Seism. Soc. Amer., 63, 157-187.

Trifunac, M. D., and V. W. Lee (1973). Routine Computer Processing of Strong Motion Accelerograms, Earthquake Eng. Res. Lab., EERL 73-03, Calif. Inst. of Tech., Pasadena.

Trifunac, M. D., and V. W. Lee (1974). A Note on the Accuracy of Computed Ground Displacements from Strong Motion Accelerograms, Bull. Seism. Soc. Amer., 64, 1209-1219.

Trifunac, M. D. (1977). Uniformly Processed Strong Earthquake Ground Accelerations in the Western United States of America for the Period from 1933 to 1971: Pseudo Relative Velocity Spectra and Processing Noise, Dept. of Civil Engr., Report No. CE 77-04, Univ. of Southern California, Los Angeles.

Trifunac, M. D. and V. W. Lee (1979). Automatic Digitization and Processing of Strong Motion Accelerograms I & II, Dept. of Civil Engr., Report No. 79-15, Univ. of Southern California, Los Angeles.

Trifunac, M. D., and V. W. Lee (1978). Uniformly Processed Strong Earthquake Ground Accelerations in the Western United States of America for the Period from 1933 to 1971: Corrected Acceleration, Velocity and Displacement Curves, Dept. of Civil Engr., Report No. CE 78-01, Univ. of Southern California, Los Angeles.